Tesis – TF142510

STUDY AND SIMULATION OF A SOLAR SYSTEM FOR DRYING PURPOSE IN RWANDA

PIERRE DAMIEN UWITIJE
NRP. 02311650027001

SUPERVISOR
Dr. Ridho Hantoro, S.T., M.T.

MASTER'S PROGRAM
EXPERTISE IN RENEWABLE ENERGY ENGINEERING
DEPARTMENT OF ENGINEERING PHYSICS
FACULTY OF INDUSTRIAL TECHNOLOGY
INSTITUT TEKNOLOGI SEPULUH NOPEMBER
SURABAYA
2018

VALIDITY SHEET

This thesis is done to fulfill one of the requirements of obtaining a degree of

Master of Engineering (M.T.)

in

Institut Teknologi Sepuluh Nopember

By:

Pierre Damien Uwitije

NRP. 02311650027001

Exam Date: 16 July 2018

Graduation Period: September 2018

Approved by:

1. Dr. Ridho Hantoro, S.T., M.T. (Supervisor)
   NIP. 19761223 200501 1 001

2. Gunawan Nugroho, S.T., M.T., Ph.D. (Examiner I)
   NIP. 19771127 200212 1 002

3. Dr.Ing. Doty Dewi Risanti, S.T., M.T., (Examiner II)
   NIP. 19740903 199802 2 001

KEMENTERIAN RISET, TEKNOLOGI, DAN PENDIDIKAN TINGGI
INSTITUT TEKNOLOGI SEPULUH NOPEMBER
FAKULTAS TEKNOLOGI INDUSTRI

Dean of Faculty of Industrial Technology,

Dr. Bambang Lelono Widjiantoro, S.T., M.T.

NIP. 19690507 199512 1 001

STUDY AND SIMULATION OF A SOLAR SYSTEM FOR DRYING PURPOSE IN RWANDA

Nama Mahasiswa	: Pierre Damien Uwitije
NRP	: 02311650027001
Pembimbing	: Dr. Ridho Hantoro, ST., MT.

ABSTRACT

Most people in developing countries obtain their income from the agriculture products but due to the lack of harvest preservation, huge losses are often observed. Obviously, the main food conservation techniques such as freezing and mechanical thermal dryers are limited by the energy demand issues. The common practiced traditional method of open sun drying sometimes fail in drying some particular products such as fruits and vegetables. This open sun method also involves a lot of risks, namely the exposure to environmental contamination, huge labour and low product quality. Development and application of improved solar systems is one of the most promising solutions.

This study provides a mathematical model and simulations for a solar collector and drying chamber of a convection indirect solar drying system designed to dry fruits and vegetables. On the basis of mass and energy balance, equations are established and solved numerically. The model used helps in studying the dynamic behaviour of system design and the effect of influential parameters on the drying process for a forced convection solar dryer with heating and without heating backup system.

Under consideration of Rwandan weather conditions, the studied system shows promising results in shortening the drying process of green pepper vegetables. The designed solar air heater shows low performance in morning hours and high performance in afternoon hours. The solar collector generates fluid output temperatures above 48^0C from 11:00 am until 6:00 pm with the highest value of

74^0C generated at 3.00pm. Inside the drying chamber, the effect of increasing drying air temperatures and velocity shortens the drying time. It is also observed that drying time for products dried in the first trays is shorter than that of products located in the last trays mainly due to the effect of temperatures distribution.

Keywords: Drying chamber, green pepper, solar collector, solar dryer modelling.

STUDY AND SIMULATION OF A SOLAR SYSTEM FOR DRYING PURPOSE IN RWANDA

Nama Mahasiswa	: Pierre Damien Uwitije
NRP	: 02311650027001
Pembimbing	: Dr. Ridho Hantoro, ST., MT.

ABSTRAK

Kebanyakan orang di negara berkembang mendapatkan penghasilan mereka dari produk pertanian tetapi setelah diamati karena kurangnya pengawetan hasik panen mengakibatkan kerugian besar. Tentunya, teknik konservasi utama untuk makanan seperti pembekuan dan pengering termal mekanik dibatasi oleh masalah permintaan energi. Metode tradisional yang dipraktekkan dari pengeringan matahari terbuka mengakibatkan kegagalan dalam pengeringan beberapa produk tertentu seperti buah dan sayuran. Metode matahari terbuka ini juga menghasilkan banyak risiko, yaitu paparan pencemaran lingkungan, kerja yang banyak dan kualitas produk rendah. Pengembangan dan penerapan sistem tata surya yang lebih baik adalah salah satu solusi yang paling menjanjikan.

Studi ini menyediakan model matematis dan simulasi untuk kolektor surya dan ruang pengering dari sistem surya konveksi yang dirancang untuk mengeringkan buah dan sayuran. Atas dasar keseimbangan massa dan energi, persamaan ditetapkan dan diselesaikan secara numerik. Model yang digunakan membantu dalam mempelajari perilaku dinamis desain sistem dan pengaruh parameter yang berpengaruh pada proses pengeringan untuk ruang pengering yang pakai sistem pemanasan dan yang tidak sistem pemanas

Dengan pertimbangan kondisi cuaca Rwanda, sistem yang diteliti menunjukkan hasil yang menjanjikan dalam mempercepar proses pengeringan sayuran lada hijau. Pemanas udara surya yang dirancang menunjukkan kinerja rendah di pagi hari dan kinerja tinggi di sore hari. Ini menghasilkan suhu output *cairan di atas* 48^0C *dari 11.00 hingga 7.00 malam dengan nilai tertinggi* 74^0C *yang dihasilkan pada 3.00PM. Di dalam ruang pengering, efek peningkatan suhu udara pengeringan dapat mempercepat waktu pengeringan. Waktu pengeringan ini lebih cepat untuk produk yang dikeringkan dalam baki pertama dibandingkan dengan produk yang terletak di bagian terakhir terutama karena pengaruh distribusi temperatur.*

Kata kunci: Ruang pengering, lada hijau, kolektor surya, pemodelan pengering matahari.

ACKNOWLEDGEMENT

I would like to take this opportunity to first and foremost thank God for giving me the strength and encouragement especially during all the challenging moments in completing this thesis.

I am deeply grateful to Dr.Ridho Hantoro, ST, MT., for having accepted to be my thesis supervisor and has orientated me in the amaizing field of solar thermal engineering. His patience, insigthful and relentless guidance contributed a lot in the completion of this thesis.

I am profoundly grateful to Dr. Gunawan Nugroho, ST, MT., PhD and Dr. Ing. Doty Dewi Risanti, ST, MT for sparing their valuable time whenever I approached them and for showing me the way ahead.

Many thanks goes to the department of engineering physics in ITS and to all lecturers for creating a friendly and encouraging academic environments. I extend my gratitude to Prof. Dr. Ir. Aulia Siti Aisjah, Dr. rer.nat. Ir. Aulia M. T. Nasution MSc., Mr. Chayun Budiono and to Mrs Martha Hardiyah for facilitating the completion of my studies.

I have great pleasure in expressing my deepest gratitude to my colleagues and fellow classmates. I convey special thanks to Wildan M., Erna S., Leonidas N., and to everyone who has been a part of my life directly or indirectly supported and prayed for me along the way.

Finally, I would like to say many thanks to the Indonesian government for the financial support, without their help it couldn’t be possible to come and study in Indonesia.

Surabaya, July 2018

Author

LIST OF CONTENTS

LIST OF FIGURES

LIST OF TABLES

NOMENCLATURE

Solar collector

Cp_g: heat capacity of glass covers (J/Kg.K)

Cp_p: heat capacity of absorber plate (J/kg.K)

Cp_i: heat capacity of insulation wall (J/kg.K)

D_f : diameter of dried product

dt: time step

h_{rgs}: Radiation heat coefficient between glass and sky.

h_{rgg}: convection heat coefficient between two glass covers.

hr_{gp}: radiation heat coefficient between second glass cover and absorber plate

$hr_{pi:}$ radiation heat coefficient between absorber plate and internal wall of insulation

hr_{is}: radiation heat coefficient between external insulation and sky.

hv: convection heat coefficient between first glass cover and sky.

hv_{gg}: convection heat coefficient between first glass and second glass

hv_{gp}: convection heat coefficient between first glass cover and plate

hv_{pf}: convection heat coefficient between absorber plate and fluid

hv_{fi}: convection heat coefficient between external insulation and sky.

hv_{is}: convection heat coefficient between external insulation and sky.

ΔS: surface of a small section

Q: mass fluid of the fluid (kg/s)

M_g: mass of each glass cover for length section ΔS

M_p: mass of absorber for length section ΔS

M_i: half of the mass of insulation for length section ΔS

P_{g1}: Power absorbed by 1 m^2 of glass (W/m^2)

P_p: Power absorbed by 1 m^2 of absorber plate (W/m^2)

Ta: Ambient temperature (K)

T_{g1}: Temperature of first glass cover (K)

T_{g1}: Temperature of first glass cover (K)

T_{g2}: Temperature of second glass cover (K)

T_p: Temperature of absorber plate (K)

Tii: Temperature of internal face of insulation (K)

T_{ie}: Temperature of external face of insulation (K)

Ts: Sky temperature (K)

Drying chamber

Cp: heat capacity of air (J/Kg.K)

Cp_f: heat capacity of products

Cp_p: heat capacity of wall face

dt: time step

h_{ce}: Convection heat coefficient between the chamber wall external face and the ambient air

$h_{cf,ach}$: convection heat coefficient between the air and the product

$h_{cd.pe}$: Conduction heat coefficient between the through the wall faces

$h_{cach.pi}$: convection heat coefficient between the air and the internal wall face

h_{re} :radiation heat coefficient between the wall external face and the sky

L_v: Evaporation latent heat of water

m_f: mass of the product

m_p: half of the wall mass

P_{ev}: evaporation power

Q: flowrate

S: exchange surface between product and air for one tray

S_p: wall face surface for one tray section

Tc: sky temperature

T_f: product temperature

T_p: temperature between two faces of the wall

T_{pi}: Internal wall face temperature

θ: heated air temperature(used for drying)

U: air speed (m/s)

This Page Is Intentionally Left Blank

CHAPTER 1
INTRODUCTION

1.1 Background

According to scientific studies, it is projected that the world population will increase to 11 billion by the end of the century [1]. To confront the immense population and resource challenges facing humanity, the provision of the adequate food supply have assumed vital importance. Modernization in farming and reduction in food losses are needed. In line with the reduction of food losses, provision of preservation techniques that optimize the factors of nutritional quality, cost and energy consumption are required. Drying is an excellent and most applicable way to preserve food products in comparison with other techniques such freezing and dehydration. Upon heating the food product during drying process, its water is transformed into vapor and the ambient air picks the moisture up and carries it away. This action of moisture content reduction impedes the development of microbial actions that are responsible for spoilage.

Traditionally, the open sun drying has been the most practiced method in many countries. In Rwanda, open sun drying is still practiced at large extent in drying most of the agriculture products. Unfortunately it is very slow due to cool ambient temperatures characterizing Rwanda. This method consists of spreading the crops thinly on raised platform or ground in the sun. Then the products are stirred and turned periodically for the adequate exposure to sunlight. Even though it is cheap and environmentally friendly, it is labor intensive and requires vast drying space. Much more it is linked to high probability of product spoilage due to long exposition to environmental contaminants. The lossmaking arising from these consequences can be substantial. In industrialized world, thermal drying is the most common method of preserving and increasing the marketability of agricultural products. Mechanical thermal dryers are energy intensive, they have a high initial and fuel running costs for motive power to drive fans and motors. The use of such systems becomes very ideal but unfortunately they are inapplicable in many places especially in the rural locations with nonexistent grid connections. Besides these limitations, if seen in the environmental point of view, their wider applications are termed with potential threat of climate change due the atmospheric pollution from the burned fossil fuels.

Indeed, it is imperative to introduce new methods that are efficient and relevant to the environment protection. Solar drying in enclosed thermal systems from the elaboration of the traditional open sun drying provides a suitable and attractive way of utilizing locally available solar energy to lower post-harvest losses. Such systems have been used elsewhere but not yet much in Rwanda. The first published study carried out in Rwanda for drying mango slices into a domestic solar dryer ascertained that this technology gives promising results in reducing food spoilage and in providing added value to the products. Obviously, the application of solar systems in Rwanda still needs a lot of studies in the development of improved and weather adoptable solar drying systems. A brief review on solar drying background and principles has been presented by Belessiotis et al. In their historic background, drying installations were found in France dating 8000 BC [2]. These were characterised by a crop paved stone using solar radiation and wind to accelerate drying process. In Africa, several attempts in developing solar dryers from local available material systems proved to be successful and helped in drying different commodities [3]. Several studies on solar drying systems and dried products showed a remarkable difference in drying time among open sun drying and different solar drying systems. In this study, the described designs include direct, indirect and mixed systems working in active or passive mode depending on the auxiliary energy source available [4].

One of the approaches to study solar drying systems and drying process in Rwanda, would be an experimental study. But though experimental studies are accurate, they tend to be very specific to one and only one product or to a particular system and are submitted to different constraints. Mainly an experimental study is limited by the capital investment, time and space. An approach to this problem, would be the use of simulators.

A simulation program is a powerful tool for system design and for studying how existing systems perform under given weather conditions. In comparison to experimental studies, simulation studies are relatively inexpensive, fast and may be used to obtain information on the effects of variables influencing the drying phenomenon [5]. Many studies involving the simulation of different solar systems and the analysis of drying processes have been carried out by different researchers in various locations [6, 7]. All these works highlight the importance of studying a solar system prior to its installation. Such a study would be an investigation of installation location external parameters as well as the effect of design materials on the drying performance. These parameters mainly include locations temperatures, location solar radiation intensity and design materials as well as the properties of the dried product [6]. If necessary, a solar drying system may be used together with a heating or without heating backup system for drying process control or for a more practical and efficient system.

1.2 Problem Formulation

Based on the background, the problem formulation of this study is as follow:

a. What is the influence of external and internal parameters on the working condition of a solar collector used in a forced convection indirect solar dryer?
b. What is the difference between using a solar dryer system with backup and using a system without backup system on the drying process?
c. What is the influence of temperature, velocity and product position on the drying process of green pepper inside an indirect dryer working at a constant temperature from morning up tonight?

1.3 Research Objectives

Based on the formulation of the problem statement, the objectives to be achieved in this study are as follows:

a. Development of MATLAB programs able to simulate the functioning of solar collectors as well as that of drying chamber under the given internal and external parameters.

b. Evaluate the difference between using a solar dryer system with backup and using a system without backup system on the drying process
c. Study the influence of external and internal parameters on the drying process of green pepper inside an indirect dryer working at a constant temperature from morning up to night

1.4 Research Limitation

During drying, heat transfer is one of the dominant phenomena. The heat is transferred in all directions between the air and products in the racks and throughout the walls of the drying boxes up to the ambient air and the sky. The developed model is based on the following simplifying assumptions:

a. The moving fluid is considered to be in one-dimension flow.
b. The temperatures of the various solid elements are considered uniform in the plane perpendicular to the air flow.
c. The physical properties of the product and constituent materials of solar system are considered constant; those of air vary with temperature and humidity.
d. The radiative exchanges inside the dryer are neglected.
e. Thermal losses and pressure drops of air moving through connector's junction are neglected
f. The heat transfer by conduction between rack and product is neglected.
g. The dried product is considered as a sphere.

1.5 Contribution

A simulation tool is a powerful tool for system design, for the development of new and improved systems and for studying existing systems under given weather conditions. The two developed Matlab programs fit well:

a. In studying the behaviors of solar air heater and drying chamber in a given environment,in this case taken as Rwanda.
b. In evaluating the influence of system design.

c. In evaluating the influence of temperature, velocity, tray position on the drying process of green pepper.

1.6 Research Methodology

This study simulate the performance of a typical convection solar dryer for drying fruits and vegetables in Rwanda. By the use of step by step model, thermal circuit analogy and drying kinetics of green pepper, analytical and numerical equations for various system elements are written and later solved numerically by Gauss Seidel method to determine the influence of geometrical design, temperature and air velocity on the system performance. The dried product is green pepper, a product of high interest largely consumed and exported in neighboring countries. To describe the mechanisms and the influence of certain process variables on the moisture transfer, an empirical power model is to describe its drying kinetics.

This Page Is Intentionally Left Blank

CHAPTER 2
LITERATURE REVIEW

2.1 Drying Principles

The concept of drying in agro-processing industry involves lowering product water content so that its water activity is brought to a lowest value allowing its conservation for longer period. The elimination or separation of water from food product can be obtained mechanically or thermaly. Several theories have been proposed to explain the drying phenomenon involving the study of mass and heat transfer in the product. Some of the most important theory include the theory of Molecular Diffusion of Liquid, theory of Capillary Mechanism, Whitaker's theory and Krischer theory [6].

The theory of Molecular Diffusion of Liquid assume that the movement of water towards the surface of the solid is governed by the Fick's law, which translates the migration phenomenon of water vapor from the middle of strong concentration of water towards the medium of low concentration of water. In other words, from within the material towards its surface. Then, on the surface, there is evaporation due to the contribution of outside energy. This theory is satisfactory for the drying of food and grains, which is not the case for other products. It is criticized for its weak representation of the physical phenomena, in the simple difference in concentration and neglect for example the temperature gradient in the solid, or put the diffusion coefficient constant, which is not valid for all products. Diffusion depends on several factors, such as the nature of the solid, and that of moisture, the humidity and temperature.

The theory of Capillary Mechanism is based on the fact that the movement of water in the pores results from a potential of suction, In the process of food drying, capillary flow, along with molecular diffusion, are considered by many scientists to be one of the main moisture transport process only at the phase where the moisture content is high. This is true for the early phases, but it is doubtful if this mechanism has a significant contribution at the later phases of drying as well.

Whitaker's Theory proposes a new way of writing heat and mass transfer equations in porous media based on the expression of heat, mass, and momentum transfer equations for each fluid phase of the material (solid, liquid, and gaseous) by setting boundary conditions at the interfaces between phases. In this theory, equations are derived for each phase in the cellular space, the intracellular space, the cell walls, and the air gaps inside the material, applying the continuity conditions at the interfaces and therefore resulting in a system of differential equations for heat and mass transfer. This approach gives useful information on the moisture and heat transfer mechanisms inside the complex structure of the food, but it is extremely difficult to apply because of the huge number of transfer coefficients and thermodynamic properties absolutely necessary for the full description of the system.

Krischer theory assumes that during drying, the moisture in the liquid state is due to the forces of capillaries, and in the vapor state is due to the concentration gradient of the vapor. Berger and Pei propose that the transfer of the liquid is due to the capillary forces and to the gradient of concentration whereas the vapor diffusion is due to the pressure gradient of the vapor.

Drying involves several parameters influencing the drying process. Mainly, the drying rate depends on the dried product properties, drying air properties as well as the heat transfer in the system. All hese studies allow to have more knowledge on the physical phenomena that occur during the drying mechanism and to interpret them in mathematical expressions reflecting reality.

2.2 Important properties of wet product

The important properties of (wet) product influencing the drying process involve the product moisture content, equilibrium moisture content and water activity [6].

The moisture content is defined as the mass of water vapor per unit mass of (dried)? product. It may be indicated as a percent or as a decimal ratio and can be expressed in two methods either wet basis or dry basis. The product moisture content in wet basis is calculated as:

$$m = \frac{m_w}{m_w + m_d} \tag{2.1}$$

In dry basis, it is determined as:

$$M = \frac{m_w}{m_d} \tag{2.2}$$

with:

m = moisture content wet basis (wb)

M = moisture content dry basis (db)

m_d = mass of dry material in the product

m_w = mass of water in the product

The product moisture content on the dry basis and wet basis are related with each other using the expression below, note that the product moisture in agriculture product is conventionally indicated in wet basis later denoted as X starting from chapter three.

$$m = \frac{M}{1 + M} \tag{2.3}$$

Product water activity is one of the important parameters in food storage stability analysis. The water activity is denoted as a_w and normally its value varies(ranges) from 0 to 1. It can be correlated with the quality and safe storage period of food products to indicate the availability of free water in a product influencing chemical reactions, growth of microorganisms and spore germinations. It may be defined as the ratio of partial pressure of water vapour just above the wet product to that of the partial pressure of pure water at the same temperature and can be controlled either by reducing moisture content which in return controls the available water content for reaction.

The equilibrium moisture content is the moisture content level where the dried product neither gains nor loses moisture since it is at equilibrium with the relative humidity of the surrounding environment. Its value depends on the product and drying physical properties, the surface-area-to-volume ratio of its shape, and the speed with which humidity is carried away or towards the material. The equilibrium moisture content (of)?(and) desorption of the product as a function of the water activity and temperature of the surrounding air, can be computed by using the well-known and widely used GAB model expressed as [7]:

$$\frac{X_{SE}}{X_M} = \frac{C\,k\,a_w}{(1 - k\,a_w)(1 - k\,a_w + C\,k\,a_w)} \tag{2.4}$$

with:

X_{SE}	= equilibrium moisture content, fraction dry basis
C	= monolayer moisture content, fraction dry basis
X_M	= Guggenheim constant
k	= factor correcting properties of multiplayer with respect to the bulk liquid,
a_w	= water activity

2.3 Important properties of wet air

The drying process is mainly characterized by the properties of air–water vapour mixture as well as many other parameters illustrated before. In the case of convective dryers, the air is heated by means of any heating source, and the hot air will be supplied to wet products to remove the moisture content. Knowledge of properties of air–water vapor mixture is imperative in the design of such solar systems and in analyzing the drying process. Some of the the preponderant properties of hot air are the dry and wet bulb temperatures, dew temperature, specific and relative humidity.

The dry bulb temperature, usually referred to as "air temperature", is the air property that is most commonly used. When people refer to the temperature of the air they are normally referring to the dry bulb temperature. the ambient air temperature measured by a thermometer which is not affected by the moisture of the air is known as dry bulb. It can be measured using a normal thermometer freely exposed to the air but shielded from radiation and moisture. If the bulb of the thermometer is wrapped with a wet tissue, then the measured temperature is referred to as wet bulb temperature. When the air is in saturated condition, the wet-bulb and dry-bulb temperatures will be equal, and in other cases, the wet-bulb temperature is less than the wet-bulb temperature. The convective drying process is almost similar to the measuring process of wet-bulb temperature. In the case of wet-bulb drying process, the bulb of thermometer is covered with a wet tissue and exposed to a moving air, whereas in convective drying process, the wet product is exposed to heated air. The knowledge of only two of these values is enough to determine the state of the moist air - including the content of water vapor and the sensible and latent energy in the air.

Water molecules escape into the overlying air volume during evaporation as surface water evaporates. Water vapor increases into air during evaporation and decreases during condensation. In a mixture of air and water vapor, the specific or saturation vapor pressure does not vary if the temperature is constant. It gives an idea of how much water the air can hold. The higher the temperature the more capacity of water that the air can hold hence it is directly related to temperature. On the other hand, the partial pressure of water vapor is related to vapor molecules in the air. When the air mixture is cooled under constant total pressure, then the partial pressure of the vapor remains unchanged but, on the other hand, the saturation vapor pressures decreases. For a certain temperature denoted as Tdp after the saturation vapor pressure becomes equal to the partial pressure of water molecules, the first traces of condensation start to occur. This Tdp temperature is referred to as dew point. The dew point temperature is the temperature at which saturation occurs in the air and is dependent upon the amount of water vapor present. Higher dew points indicate abundant atmospheric moisture.

The Specific humidity represents a mass of water vapor per unit of dry air in the mixture of vapor and air. It is expressed as grams of water vapor per kg of dry air. It can be calculated from the mass of water m_w and from the mass of dry air m_a as follows [6]:

$$H = \frac{m_w}{m_a} \tag{2.5}$$

It can also be calculated in the case of wet air from the total pressure P_t of air and water mixture and from the partial pressure of water vapor P_w as:

$$H = 0.622\left(\frac{P_w}{P_t - P_w}\right) \tag{2.6}$$

Relative humidity RH is the relative amount of water vapor to the maximum that can exist at a particular temperature. It is calculated from the partial pressure of water vapor at a given temperature P_w and from partial pressure of water vapor at saturation at the same temperature.

$$RH = \frac{P_w}{P_{ws}} * 100 \tag{2.7}$$

2.4 Drying Kinetics

Drying kinetics defines the changes of average product moisture content and average temperature with time in a drying body. The knowledge in drying kinetics of a product can be applied in calculating the amount of moisture evaporated, drying time, energy consumption and other related parameters. It is considered as a very important parameter as it is used for the design and simulation of dryer. The drying kinetics completely explains the transport properties such as mass transfer coefficient, moisture diffusion, heat transfer, etc. involved in the drying process. Drying kinetics may be defined as the dependence of factors affecting drying and drying rate. These models consider various factors including air properties, type and size of the product and drying system. Based on this, drying process is classified into thin layer solar drying and deep bed drying models. In deep bed, products drying is done in zones forming a big and wide layer. During the drying a gradient of temperature and humidity is observed between the lower and upper zones. Generally, the deep bed simulation proves to be very complex as various changing parameters are involved in the process. To facilitate this task, deep bed can be considered as the superposition of many thin layers. The thin layer is used for lab test to find drying constants or to rewrite an empirical equation. It assumes that the ratio of the drying air volume compared to product volume is very large or that the drying layer within which all product have almost the same exposure. In view of this supposition, drying rate is influenced simply by the product properties and size, drying air temperature and moisture content. Thin layer drying equations may be of theoretical, semi theoretical or empirical equations [6].

The theoretical models have been derived by considering the internal resistance to moisture transfer, and they explain the drying behavior of the product at all conditions. The widely used theoretical models are derived from Fick's second law of diffusion. For example, Table 2.1 represents some of the thin layer models derived from this Fick's second law of diffusion.

Table 2. 1 Thin layer models derived from Fick's second law of diffusion

Name of the model	Model	References
Henderson and Pabis (single-term) model	$MR = a\exp(-kt)$	Henderson and Pabis (1961)
Logarithmic or (asymptotic) model	$MR = a\exp(-kt) + c$	Chandra and Singh (1984)
Midilli model	$MR = a\exp(-kt) + b^{*}t$	Midilli et al. (2002)
Modified Midilli model	$MR = \exp(-kt) + b^{*}t$	Ghazanfari et al. (2006)
Demir et al. Model	$MR = a\exp[(-kt)] + b$	Demir et al. (2007)
Two term model	$MR = a\exp(-k_1t) + b.\exp(-k_2t)$	Henderson (1974)
Two term exponential model	$MR = a\exp(-kt) + (1-a)\exp(-kat)$	Sharaf-Eldeen et al. (1980)
Modified two term exponential models – Verma model	$MR = a\exp(-kt) + (1-a).\exp(-gt)$	Verma et al. (1985)
Modified Henderson and Pabis (three term exponential) model	$MR = a\exp(-kt) + b.\exp(-gt) + c\exp(-ht)$	Karathanos (1999)

There are also semi-theoretical models derived from Fick's second law and Newton's law of cooling. As an example Table 2.2 shows the thin layer model derived from Newton's law of cooling. Lastly, there are empirical models derived from experiments. The most used empirical models for thin layer are shown in Table 2.3.

Table 2. 2 The models derived from Newton's law of cooling

Name of the model	Model	References
Lewis (Newton) model	$MR = ep(-kt)$	Lewis (1921)
Page model	$MR = \exp(-kt^n)$	Diamante and Munro (1993)
Modified page-I models	$MR = \exp(-kt)^n$	Overhults et al. (1973)
Modified page-II models	$MR = \exp - (kt)^n$	White et al. (1978)

Table 2. 3 Empirical models

Name of the model	Model	References
Thompson model	$t = a\ln(MR).b.[\ln(MR)]^\wedge 2$	Thompson et al. (1968)
Wang and Singh model	$MR = 1 + b^*t + a^*t^2$	Wang and Singh (1978)
Kaleemullah model	$MR = \exp(-c^*T) + b^*.t^{(pT+n)}$	Kaleemullah and Kailappan (2006)

2.5 Overview on solar dryers

Solar drying is mainly classified into two main methods. The first type is known as conventional open sun drying; it is characterized by the spreading of products on the ground or raised bed under the sun. In the second solar drying type, products are kept inside a system called solar dryer. The use of solar dryer rather than open sun conventional method is termed with some advantages such as small area requirement for drying large product quantities. In addition, the yielded dried product is of high quality because molds, rodents are unlikely to infest the product during drying process. Once again, the drying period is shortened and products are protected from sudden rainfalls and wind resulting in less labor for farmers. Solar dryers are categorized generally into four types namely known as direct, indirect, mixed mode solar dryer and hybrid solar dryer [8] as shown in figure 2.1.

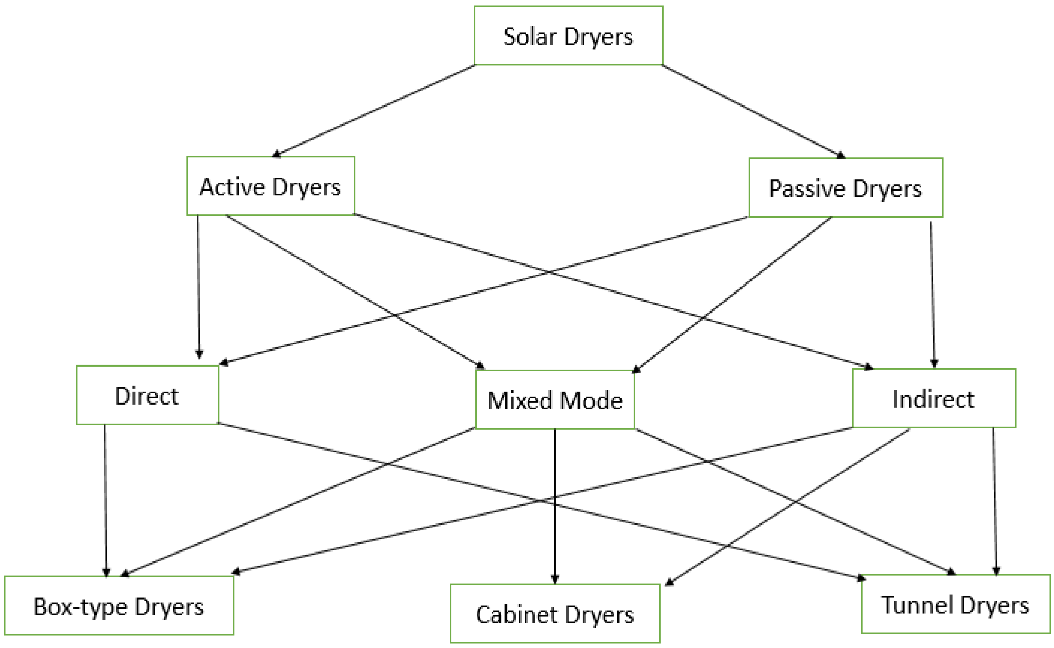

Fig. 2. 1 Solar dryer classifications [8]

Starting from the direct solar dryer, product dried in this system are directly exposed to sunlight. Thus, direct solar dryers rely on the sunlight direct conversion process. To enhance solar radiation conversion into thermal energy, the system is constituted by container painted black and may be given a glass lid cover and some vents for efficiency improvement. Direct solar dryer systems have three different types including box, cabinet and tunnel types. Extra solar radiations reduce the quality of food and the color changes.

Secondly, for indirect solar dryer systems the product has no direct contact with solar radiation. A hot air is subsequently sent in the drying chamber where the products are located. The air is heated either by solar collector systems and is blown either naturally or by force into the drying chamber. To enhance the moisture removal, the chamber is given an air vent at the top portion. The drying quality of this system is better compared to direct dryers.

Next, mixed-mode solar dryer combines direct and indirect thermal conversion types. The dried product exposure to solar radiation and furnished heated air accelerate the drying process hence this method is the most efficient for product with higher moisture content. Lastly, regarding hybrid dryers, the drying process depend both on the solar energy and on other energy sources. Mainly, the second energy source is used to heat the ambient air and to operate the blower. This system offers favorable drying condition, moreover the process can be well controlled efficiently which further results in better dried product quality.

2.6 Overview on solar collectors

Solar collectors are systems that capture and transform the energy of the solar radiation in thermal energy. There is a wide range of solar collectors that can respond to different heating needs of liquids. Their choice depends on the temperature of interest and the climatic conditions during the period of use of the system. The more temperature level is need, the more advanced technologies are implemented and the higher is cost for its production. In principle, solar collectors can be divided into two types of flat and concentrator solar collectors. Flat collectors may in turn be classified depending on the number or absence glazing system or depending on the absorber shape [9]. Cold countries generally require high-performance devices that require equipping the collector by double glazing or by an anti-reflective layer on the cover. Another method maybe the use of selective coating on the absorber that only re-emits a small portion of the energy absorbed or by using an elaborated absorber shape increasing the convective heat transfer coefficient. The essential characteristics of a glazing are the high transmission coefficient (τ) and low emissivity (ε).The absorber plays the main role in the flat solar collector, a good one must have characteristics of good absorption coefficient, good thermal conductivity, and good resistance to corrosion. The choice of material and the method of construction has a great influence on the quality of the collector. Due to their high conductivities, the absorbers are generally made in copper, steel or aluminum [10].

2.7 Related previous work on solar modelling

In general the simulation and analysis of solar drying system involve a lot of various approaches. Mainly they may be categorized into differential equation-based, statistics-based modeling, reacting engineering approach method and thermodynamic modeling. In the differential equation approach, the governing equations for all parts of the system to obtain temperature, velocity, and humidity profiles by the use of CFD method, it has an advantage of studying complex geometries but it is also restricted by large number of calculations. The statistical methods are mostly used to derive the equations based on a series of experimental data and to judge them based on different criteria to find an equation capable of describing well the behavior of the system. Reacting engineering approach follows the basic rules of chemical reaction engineering to model the kinetics of drying. In thermodynamic modeling,which is the modelling approach used in this study, a state equation is solved for all parts of the dryer to determine the temperature, pressure, and velocity. This method is fast, and if semi empirical equations are used, more accurate results can be achieved, its disadvantage is its tendency to neglect some parameters involving geometric complexity. The development of simulation structures adequate for practical use is carried out with different methodologies, depending on the objectives of the modeling process as well as on the available information.

In the following section, we present the main researches that has addressed the thermodynamic simulation of solar dyers, mainly an attention is made on convection solar drying systems. In all these works, the researchers’ motivation and contribution are driven by the benefits of solar dryers which are mainly the character of using renewable energy namely the solar energy.

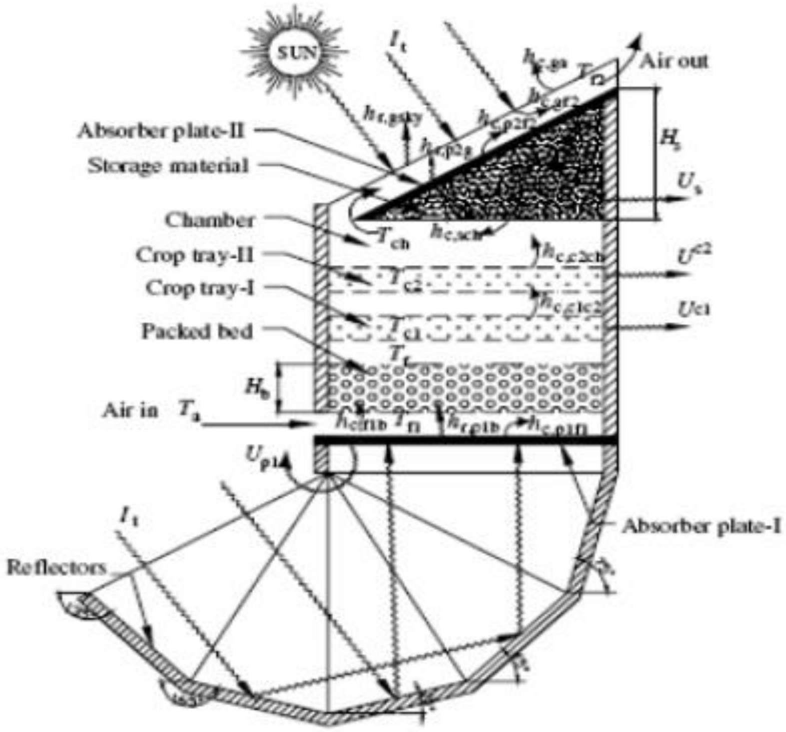

Fig. 2. 2 Solar dryer with heat storage and reflectors [11]

Dilip Jain in 2005 developed a new type of natural convection solar crop dryer having a reversed absorber plate type with a thermal storage which ensures warm air during the non-sunny period. The representation of his solar dryer is shown in Fig. 2.2. He studied such a system using a transient analytical model and used the drying characteristics of onions to evaluate the system's drying performance. The transient model was solved considering a day of October under the climatic condition of Delhi. The intensity of solar radiation and ambient temperatures estimated is shown in Fig. 2.3. With these inputs, a solar collector with reversed absorber plate of 1 m length and 1 m breadth with 0.15 m packed storage bed could dry 95 kg of onion from a moisture content of 6.14–0.27 kg water/kg of dry matter in a 24 h drying period. In his calculations, a computer program was made to solve the energy balance equation on different system components and to compute the air temperatures and various functional components of the drying system. Mainly the parametric study involved the effect of width of airflow channel and height of packed bed on the crop temperature [11].

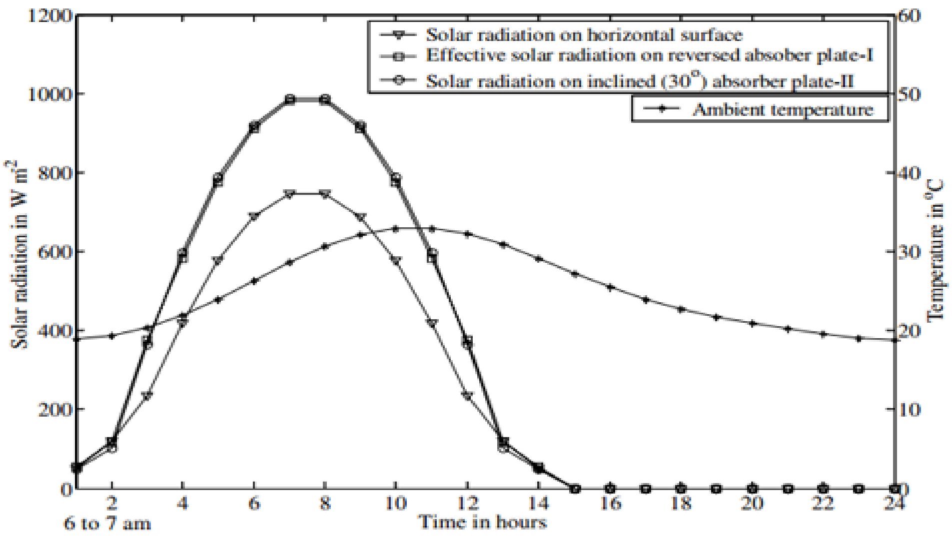

Fig. 2. 3 Average hourly ambient and solar intensity on different surfaces [11]

In 2012 Yolanda et al made a study on crop solar dryer from the fundamental point of view up to the importance and development of agricultural models and the increasing necessity in decision support systems for solar dryer designers. In this line of facilitating decision support in designing a solar dryer, they have developed an interactive program in the idea of helping the task of simulating a multi trays mixed mode solar dryer system. Their modeling was based on establishing and solving energy balance equations of all subparts of the solar air heater, drying chamber trays and storage material. The program was coded using easy Java tool. In their program, parameters might be changed in order to specify the optimal values. Using this tool, the temperatures of different trays, the moisture content and the drying rate could be predicted for different products. The modelled system involved a solar collector, a storage material and multi trays in the drying chamber. This model was tested and validated by real solar dryer system and showed to perform very well [1].

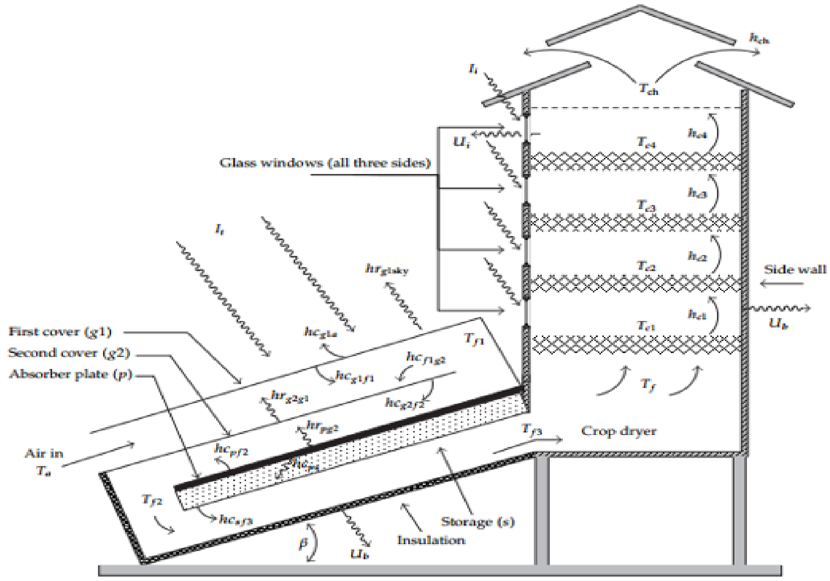

Fig. 2. 4 Multi-tray crop dryer with inclined multi-pass air heater with built thermal storage [12].

An almost similar multi-tray crop drying attached to an inclined multi pass solar air heater within built thermal storage was studied and modelled before in 2005 by Dilip Jain who evaluated its thermal periodic analysis and its hourly system performance for drying paddy crop. The parametric analysis of the system involved the effect of change in the tilt angle, length and breadth of a collector and mass flow rate on the temperature of crop. The hourly reduction in moisture content of products and drying rate in the different trays with the optimum parameters of the solar air heater as shown in Fig.2.4. Different reduction in moisture content has been observed in different drying trays due to the variation in crop temperatures. It has been observed that the paddy moisture content decreases with the drying time of the day. In summary the proposed model was useful for evaluating the thermal performance of a flat plate solar air heater and could be used at designing and developing tool used to study and forecast the behavior of paddy drying process inside a multi -tray solar dryer [13].

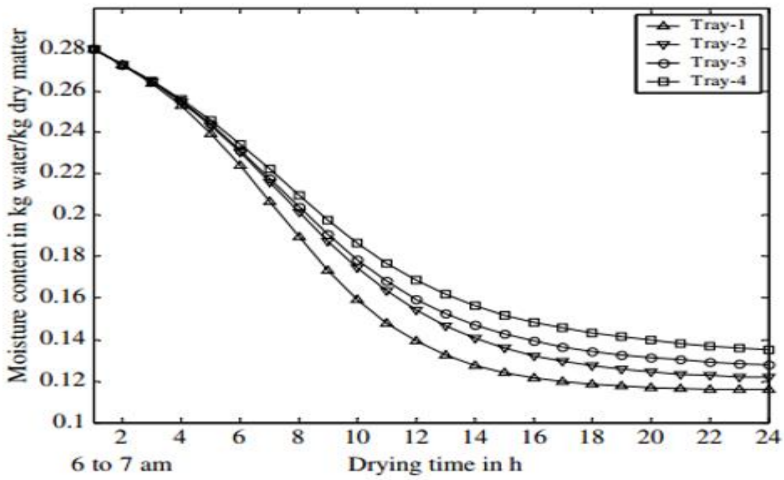

Fig. 2. 5 Variation of moisture content with drying time in four trays [12]

In the research done by Nasri et al, a solar collector as well as drying chamber of a forced convection indirect solar dryer system working to dry fruits and vegetables were modelled and simulated. The results from the parametric study on the collector could describe the hourly variation of all solar collector components as shown in Fig. 2.6. The simulated single-glazed solar air collector was carried out by solving the thermodynamic equations established from the energy balance on different components by using Gauss Seidel method [13].

Previously in the study done by Bennamoun et al. on a similar system amazing results on the drying process of onions were presented. The increase of drying air happened to be the most influential parameter conducting to short drying time as shown in Fig 2.7. They showed the influence of drying on using a solar dryer with backup and non-backup system. The improvements done on system after adding a backup system resulted in a quick and short drying rate [14].

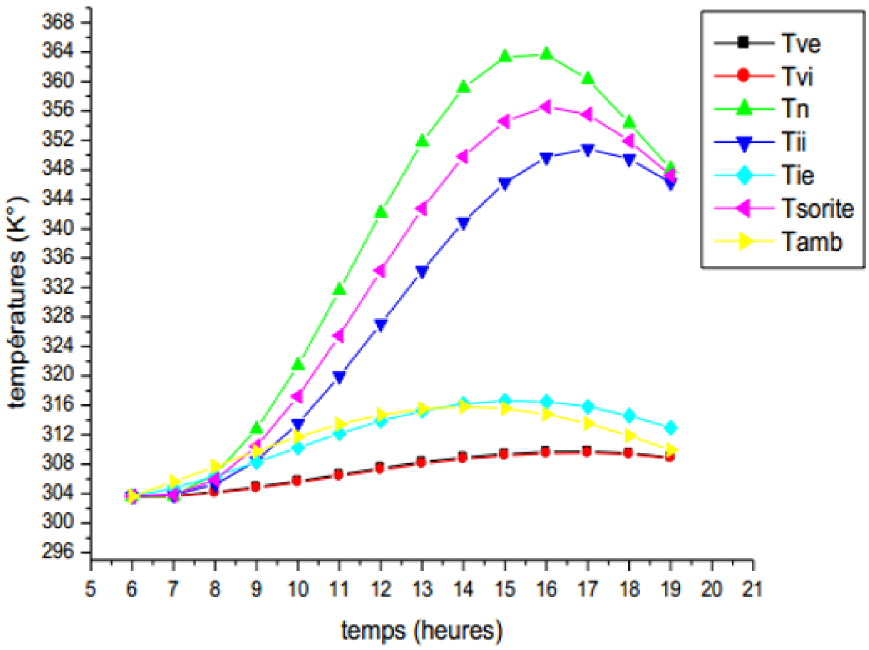

Fig. 2. 6 Variation in temperatures for different solar collector elements [13]

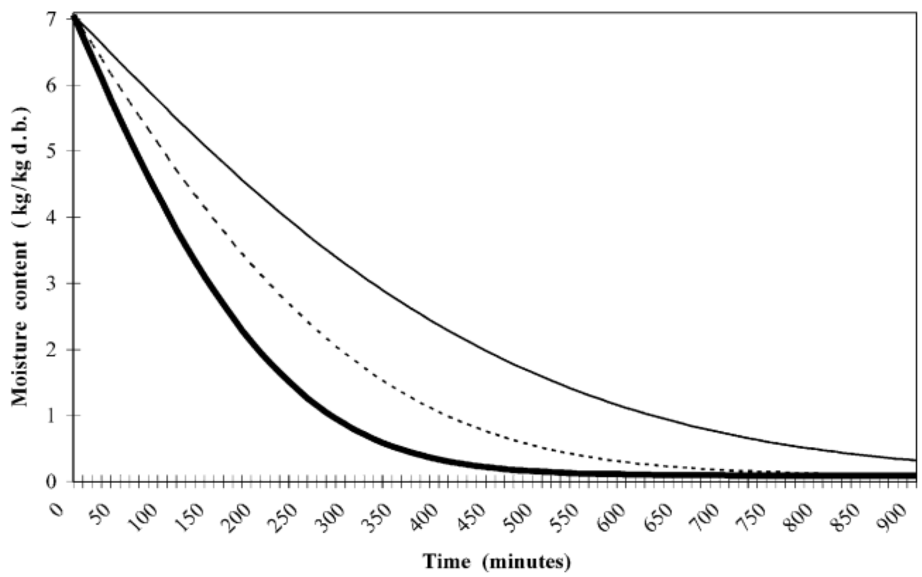

Fig. 2. 7 Effect of drying at varying temperatures and constant temperatures maintained by the backup system [14]

CHAPTER 3
RESEARCH METHODOLOGY

3.1 Presentation of the dryer

The drying system used in this study is shown in Fig. 3.1 representing a typical indirect convection dryer designed to dry fruits and vegetables [13]. It consists of two main parts, a double glazed conventional solar air heater and a drying chamber. The collector is tilted at 15^0 with respect to the horizontal. On its top, it consists of two glass covers spaced by 15 mm with a thickness of 10 mm. In the middle, a galvanized sheet painted black of thickness 1 mm is used as an absorber whereas at the bottom it has a polystyrene insulation of 4 cm thick.

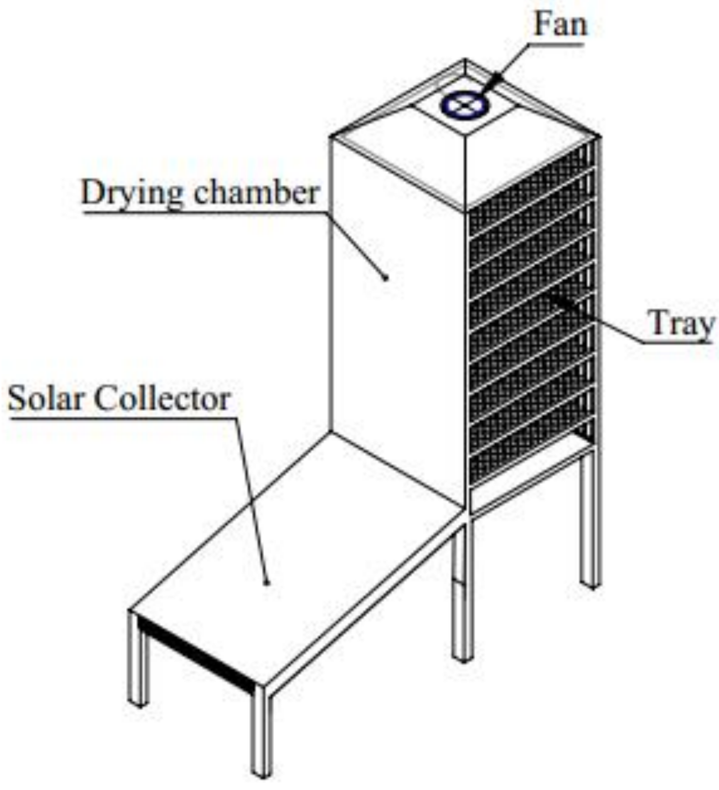

Fig. 3. 1 Studied and simulated solar dryer system

The drying chamber is a cubic box of small dimensions whereas the height is 1m, width is 1m and the depth is equal to1m. The simulated material constituting the dryer chamber is the solid clay brick of thickness of 10 cm with external insulation made of polystyrene 4 cm thick to minimize the exchange of heat with the external environment. The dryer has 10 trays, on which are laid the products to dry. The trays are distant from each other by 10 cm happening to be an enough space for the smooth air circulation. A fan is also used (placed) at the rooftop of the dryer to ensure forced convection.

Table 3. 1Solar dryer system specifications and measurements

Solar Collector type	Conventional solar collector
Overall Dimension	2.5m x 1m
No. of glazing	2 normal window glass (thickness 10 mm)
Absorber Material	Aluminium painted black (thickness 1mm)
Back insulation	polystyrene (thickness 40mm)
Collector tilt angle	15^0
Drying chamber	1 m x 1 m x 1 m
No. of trays	10 trays
Dried product	Green pepper

3.2 Formulation of calculation Method.

During drying, heat transfer is one of the dominant phenomena. The heat is transferred in all directions between the air and products in the racks and throughout the walls of the drying boxes up to the ambient air and the sky.

The developed model is based on the following simplifying assumptions:

- The moving flid is considered to in one-dimension flow
- The temperatures of the various solid media are uniform in one plane perpendicular to the flow.
- The physical properties of the product and constituent materials the solar collector and the dryer are constant; those of air vary with temperature and humidity.
- The radiative exchanges inside the dryer are neglected.

- Thermal losses and pressure drops of air moving through junction connectionare are neglected
- The heat transfer by conduction between racks and product is neglected.
- The dried product is considered as a sphere.

The thermal analysis for solar collector and drying chamber component and air streams, will be carried out considering the first principle of thermodynamics for energy and mass rate conservation saying that energy stored in the element is equal to the energy it received by conduction, radiation and convection minus the energy it lost by conduction, convection and radiation.

The heat conduction is observed in the solid medium making the dryer. It's the transfer case in the walls of the dryer and inside the solar collector layers. This heat transfer is a very important factor in the design and optimization of a dryer, it determines the quantity of heat drained outwards which in turn influences the thermal losses of the dryer and its performance. The choice of dryer wall material depends on the coefficient of material conductivity. A material having a high conductivity coefficient is not suitable for an efficient dryer. The thermal conductivity in an element of area (surf) and thickness (dx) considered as a rectangle is calculated according to Fourier's law of conduction as [15]:

$$q = -k * \mathrm{surf} * \frac{dT}{dx} \tag{3.1}$$

Inside the dryer, heat transfer between air and product, air and walls, air and racks, is done by convection. This is the most interesting mode of heat transfer in which the drying air moves around the dried product. Heat transfer by convection is also noticeable outside the dryer, between the walls external and ambient air. The convective rate of heat transfer between a solid surface and a fluid with a convective heat transfer coefficient h_c and temperature difference ΔT may be described as [15].

$$q_c = h_c\, A\, \Delta T \tag{3.2}$$

Lastly, the most dominant heat transfer mode in the case of solar dryers is radiant heat transfer. It takes into account the exchange between the outer wall of the dryer and the sky, and the exchange between the upper part of collector and the sky. The radiation heat exchange rate between two surfaces of temperature T_1 and T_2 with the radiative heat transfer coefficient h_r is expressed as [15].

$$q_{rad} = h_r \, A \, \Delta T \tag{3.3}$$

The heat Q gained or lost by any component in the dryer from the drying medium to increase or reduce its heat content without changing the product state is calculated as [15]:

$$Q = m \, . \, C \, . \, (T_2 - T_1) \tag{3.4}$$

Where

m: Product mass (kg),

C: Specific heat (kJ/kg K)

3.3 Calculation Method

In this study, the system is studied performing unsteady state analysis to gain lots of useful information. Transient or unsteady heat transfer considers that phase when the temperature changes as a function of both location and time. By contrast, in steady-state heat transfer, temperature changes only with location. initial unsteady-state period, many important responses may take place [15]. Therefore, analysing the temperature variations with time during the transient period is essential in designing a drying process.

In modelling the solar air heater, mainly the global modelling by Hottel, Whillier and Bliss and the step by step approach proposed by Michel Daguenet are followed. In comparison with the first one assuming that the regime is permanent and the collector elements are each at an average constant temperature hence neglecting the effects of thermal inertia, we have adopted the step by step mathematical model accounting for the evolution of temperatures of all solar air heater elements in time and space while involving the effects of thermal inertia. Such a method consist of taking successively short section in the direction of air flow and establishing heat and mass balance for each section [16]

3.4 Energy balance for solar collector

Our choice for using the double cover solar air heater was based on its capacity to generate high temperature while working in cool ambient temperatures compared to the single pass collector. Establishing heat and mass balance for each section considered based on the thermal circuits shown in Fig.3.2.

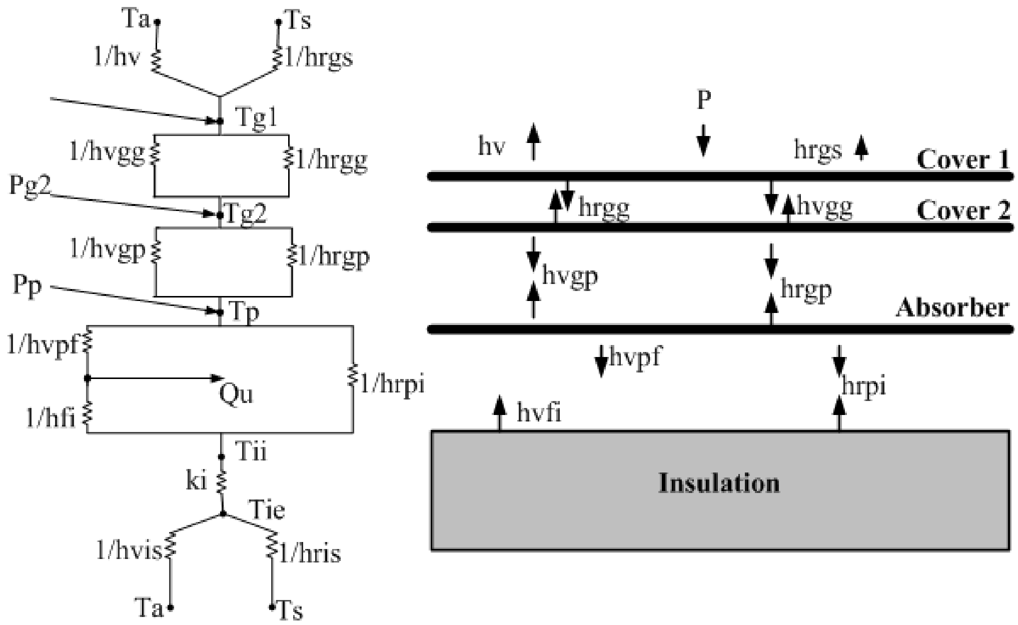

Fig. 3. 2 Thermal circuit of double glazed conventional solar collector

The energy balance for solar air heater element taken as a node is as follow:

For the first glass cover:

$$\frac{M_{g1}.Cp_{g1}}{\Delta S}\left(\frac{dT_{g1}}{dt}\right) = P_{g1} + hr_{gs}(Ts - T_{g1}) + hv\,(Ta - T_{g1}) + hv_{gg}(T_{g2} - T_{g1}) + hr_{gg}\,(Tg_2 - T_{g1}) \tag{3.5}$$

For the second glass cover:

$$\frac{M_{g2}.Cp_{g2}}{\Delta S}\left(\frac{dT_{g2}}{dt}\right) = P_{g2} + hv_{gg}(T_{g1} - T_{g2}) + hr_{gg}(T_{g1} - T_{g2}) + hv_{gp}(T_p - T_{g2}) + hr_{gp}(T_p - T_{g2}) \tag{3.6}$$

For the absorber plate:

$$\frac{Mp.Cp_p}{\Delta S}\left(\frac{dT_p}{dt}\right) = P_p + hv_{gp}\left(T_{g2} - T_p\right) + hr_{gp}\left(T_{g2} - T_p\right) + hv_{pf}\left(T(j-1) - T_p\right) + hr_{pi}\left(Tii - T_p\right) \tag{3.7}$$

For the internal part of the insulation:

$$\frac{Mii.Cpi}{\Delta S}\left(\frac{dTii}{dt}\right) = hv_{fi}(T(j-1) - Tii) + hr_{pi}\left(T_p - Tii\right) + hci(Tie - Tii) \tag{3.8}$$

For the external part of the insulation

$$\frac{Mie.Cpie}{\Delta S}\left(\frac{dTie}{dt}\right) = hci(Tii - Tie) + hv_{is}(Ta - Tie) + hr_{is}(Ts - Tie) \tag{3.9}$$

And finally, for the air flow stream as:

$$\frac{Q.Cp_f}{\Delta S}\left(T(j) - T(j)\right) = hv_{fp}\left(T_p - T(j-1)\right) + hv_{fi}\left(Tii - T(j-1)\right) \tag{3.10}$$

At this level, finite difference method is applied to discretize in time and space the set of six equations obtained from the energy balance of solar air heater parts.

For the first glass cover:

$$\frac{M_{g1}.Cp_{g1}}{\Delta S\,\Delta t}\left(T_{g1}^{t+\Delta t}(j) - T_{g1}^{t}(j)\right) = P_{g1} + hr_{gs}\left(Ts - T_{g1}^{t+\Delta t}(j)\right) + hv\left(Ta - T_{g1}^{t+\Delta t}(j)\right) + hv_{gg}\left(T_{g2}^{t+\Delta t}(j) - T_{g1}^{t+\Delta t}(j)\right) + hr_{gg}\left(Tg_{2}^{t+\Delta t}(j) - T_{g1}^{t+\Delta t}(j)\right) \tag{3.11}$$

For the second glass cover:

$$\frac{M_{g2}.Cp_{g2}}{\Delta S\,\Delta t}\left(T_{g2}^{t+\Delta t}(j)-T_{g2}^{t}(j)\right)$$
$$=P_{g2}+hv_{gg}\left(T_{g1}^{t+\Delta t}(j)-T_{g2}^{t+\Delta t}(j)\right)$$
$$+hr_{gg}\left(T_{g1}^{t+\Delta t}(j)-T_{g2}^{t+\Delta t}(j)\right) \quad (3.12)$$
$$+hv_{gp}\left(T_{p}^{t+\Delta t}(j)-T_{g2}^{t+\Delta t}(j)\right)$$
$$+hr_{gp}\left(T_{p}^{t+\Delta t}(j)-T_{g2}^{(t+\Delta t)}(j)\right)$$

For the absorber plate:

$$\frac{Mp.Cp_{p}}{\Delta S}\left(T_{p}^{t+\Delta t}(j)-T_{p}^{t}(j)\right)$$
$$=P_{p}+hv_{gp}\left(T_{g2}^{t+\Delta t}(j)-T_{p}^{t+\Delta t}(j)\right)$$
$$+hr_{gp}\left(T_{g2}^{t+\Delta t}(j)-T_{p}^{t+\Delta t}(j)\right) \quad (3.13)$$
$$+hv_{pf}\left(T^{t+\Delta t}(j-1)-T_{p}^{t+\Delta t}(j)\right)$$
$$+hr_{pi}\left(Tii^{t+\Delta t}(j)-T_{p}^{t+\Delta t}(j)\right)$$

For the internal part of the insulation:

$$\frac{Mii.Cpi}{\Delta S}\left(T_{ii}^{t+\Delta t}(j)-T_{ii}^{t}(j)\right)$$
$$=hv_{fi}\left(T^{t+\Delta t}(j-1)-T_{ii}^{t+\Delta t}(j)\right) \quad (3.14)$$
$$+hr_{pi}\left(T_{p}^{t+\Delta t}(j)-T_{ii}^{t+\Delta t}(j)\right)+hci\left(T_{ie}^{t+\Delta t}-T_{ii}^{t+\Delta t}(j)\right)$$

For the external part of the insulation

$$\frac{Mie.Cpie}{\Delta S}\left(T_{ie}^{t+\Delta t}(j)-T_{ie}^{t}(j)\right)$$
$$=hci\left(T_{ii}^{t+\Delta t}(j)-T_{ie}^{t+\Delta t}(j)\right)+hv_{is}(Ta-T_{ie}^{t+\Delta t}(j)) \quad (3.15)$$
$$+hr_{is}\left(Ts-T_{ie}^{t+\Delta t}\right)$$

And finally, for the air flow stream as:

$$\frac{Q.Cp_{f}}{\Delta S}\,(T^{t+\Delta t}(j)-T^{t+\Delta t}(j-1))=hv_{fp}\left(T_{p}^{t+\Delta t}(j)-T^{t+\Delta t}(j-1)\right)+ \quad (3.16)$$
$$hv_{fi}\left(T_{ii}^{t+\Delta t}(j)-T^{t+\Delta t}(j-1)\right)$$

with:

$$\Delta S = \mathrm{width} \, . \, \Delta x \tag{3.17}$$

where:

Δx = Length of section

From these equations, a matrix system of equation may be derived and written in the following form:

$$\begin{bmatrix} C_{11} & C_{12} & C_{13} & C_{14} & C_{15} & C_{16} \\ C_{21} & C_{22} & C_{23} & C_{24} & C_{25} & C_{66} \\ C_{31} & C_{32} & C_{33} & C_{24} & C_{35} & C_{66} \\ C_{41} & C_{42} & C_{43} & C_{24} & C_{45} & C_{66} \\ C_{51} & C_{52} & C_{53} & C_{24} & C_{55} & C_{66} \\ C_{61} & C_{62} & C_{63} & C_{24} & C_{56} & C_{66} \end{bmatrix} \times \begin{bmatrix} T_{g1}^{t+\Delta t}(j) \\ T_{g2}^{t+\Delta t}(j) \\ T_{p}^{t+\Delta t}(j) \\ T_{ii}^{t+\Delta t}(j) \\ T_{ie}^{t+\Delta t}(j) \\ T^{t+\Delta t}(j) \end{bmatrix} = \begin{bmatrix} D_1 \\ D_2 \\ D_3 \\ D_4 \\ D_5 \\ D_6 \end{bmatrix} \tag{3.18}$$

With the following entries:

First line of the matrix system

$$C_{11} = \frac{M_{g1} \, . \, Cp_{g1}}{\Delta t . \Delta S} + hr_{gs} + hv + hr_{gg} + hv_{gg} \tag{3.19}$$

$$C_{12} = -(hr_{gg} + hv_{gg}) \tag{3.20}$$

$$D_1 = P_{g1} + hr_{gs} \, . \, Ts + hv \, . \, Ta + \frac{M_{g1} \, . \, Cp_{g1}}{\Delta t \, . \, \Delta S} \, . \, T_{g1}^{t}(j) \tag{3.21}$$

Second line of the matrix system

$$C_{21} = -\left(hr_{gg} + hv_{gg}\right) \tag{3.22}$$

$$C_{22} = \frac{M_{g2} \, . \, Cp_{g2}}{\Delta t . \Delta S} + hr_{gg} + hv_{gg} + hr_{gp} + hv_{gp} \tag{3.23}$$

$$C_{23} = -(hr_{gp} + hv_{gp}) \tag{3.24}$$

$$D_2 = P_{g2} + \frac{M_{g2} \, . \, Cp_{g2}}{\Delta t \, . \, \Delta S} \, . \, T_{g2}^{t}(j) \tag{3.25}$$

Third line of the matrix system

$$C_{32} = -\left(hr_{gp} + hv_{gp}\right) \tag{3.26}$$

$$C_{33} = \frac{M_{p} \, . \, Cp_{p}}{\Delta t \, . \, \Delta S} + hr_{gp} + hv_{gp} + hr_{pi} + hv_{pf} \tag{3.27}$$

$$C_{34} = -hr_{pi} \tag{3.28}$$

$$D_3 = P_p + hv_{pf} \,.\, T^{t+\Delta t}(j-1) + \frac{M_p \,.\, Cp_p}{\Delta t \,.\, \Delta S} \,.\, T_p^t(j) \tag{3.29}$$

Fourth line of the matrix system

$$C_{43} = -hr_{pi} \tag{3.30}$$

$$C_{44} = \frac{M_{ii} \,.\, Cp_{ii}}{\Delta t \,.\, \Delta S} + hr_{pi} + hv_{fi} + hci \tag{3.31}$$

$$C_{45} = -hci \tag{3.32}$$

$$D_4 = hv_{fi} \,.\, T^{t+\Delta t}(j-1) + \frac{M_{ii} \,.\, Cp_{ii}}{\Delta t \,.\, \Delta S} \,.\, T_{ii}^t(j) \tag{3.33}$$

Fifth line of the matrix system

$$C_{55} = \frac{M_{ie} \,.\, Cp_{ie}}{\Delta t \,.\, \Delta S} + hci + hr_{is} + hv_{is} \tag{3.34}$$

$$D_5 = hr_{is} \,.\, Ts + hv_{is} \,.\, Ta + \frac{M_{ie} \,.\, Cp_{ie}}{\Delta t \,.\, \Delta S} \,.\, T_{ie}^t(j) \tag{3.35}$$

Sixth line of the matrix system

$$C_{63} = -hv_{pf} \,.\, \Delta S \tag{3.36}$$

$$C_{64} = -hv_{pf} \,.\, \Delta S \tag{3.37}$$

$$C_{66} = Q \,.\, Cp_f \tag{3.38}$$

$$D_6 = Q \,.\, Cp_f \,.\, T^{t+\Delta t}(j-1) + 2 * hv_{pf} \,.\, T^{t+\Delta t}(j-1) \tag{3.39}$$

After we are ready to solve each set of obtained equations into a matrix system of$[A][T] = [B]$, $[T]$ represents the vector of the six unknown quantities for the collector. Later a Matlab program is developed where the iterative Gauss–Seidel Method is used to solve the system of equations.

Flowchart for the solar collector simulation program

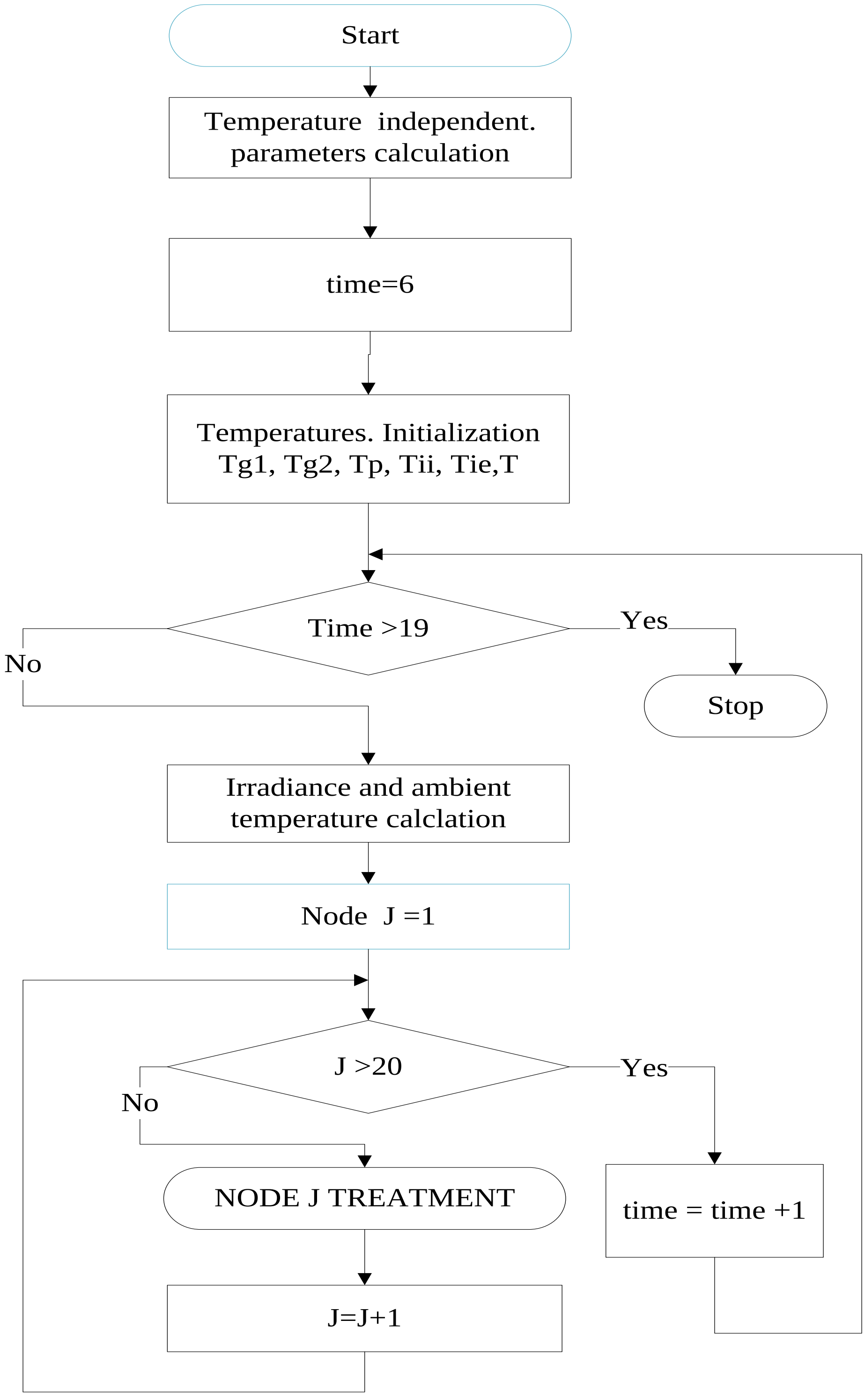

Fig. 3. 3 Flowchart for solar collector simulation program

<u>Flowchart for nodes J treatment</u>

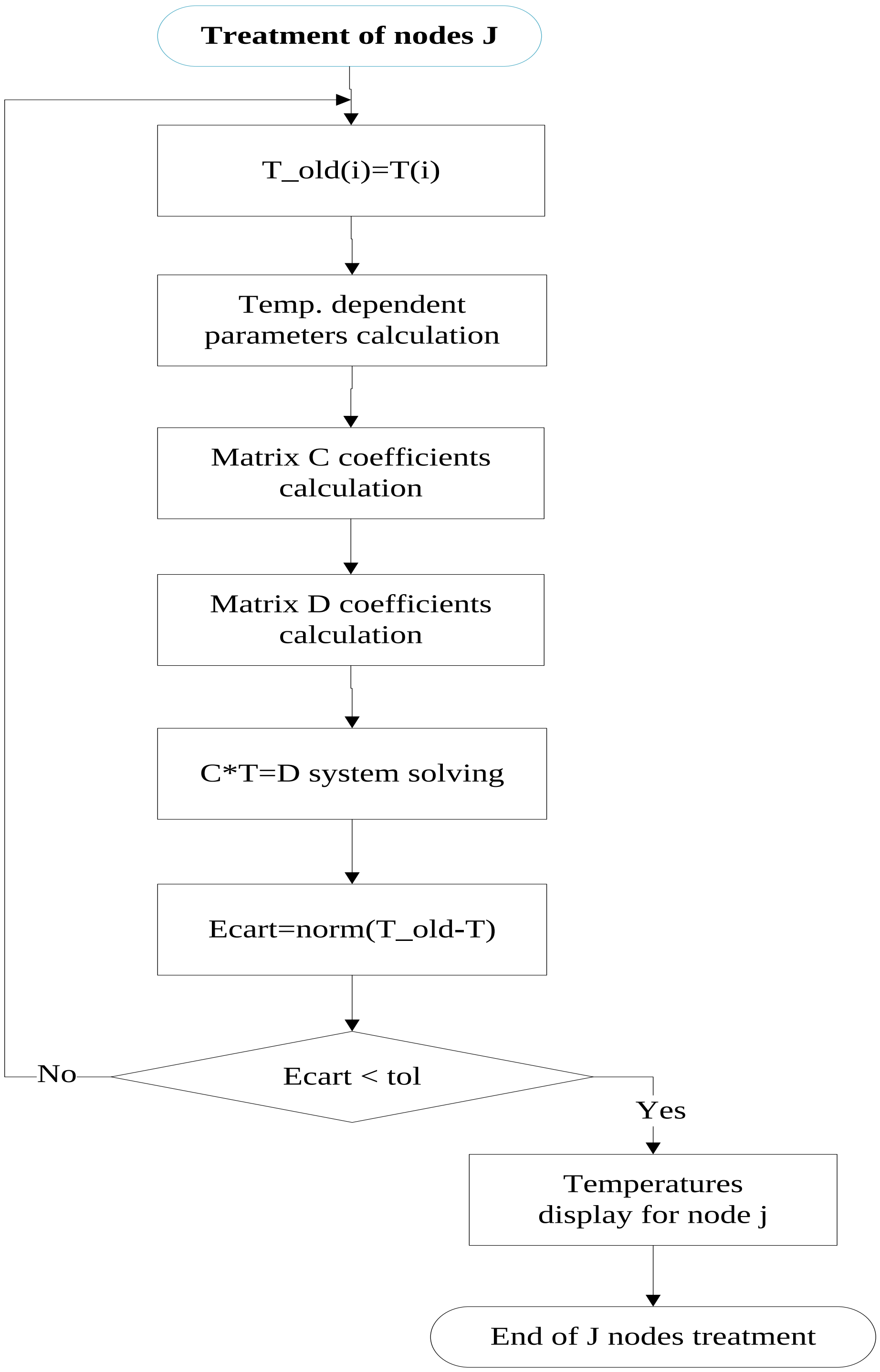

Fig. 3. 4 Flowchart for J nodes treatment in solar collector program

3.4.1 Simulation flowchart for the solar collector

Fig.3.3 represents the flowchart of the program developed for numerical calculation. At the initial moment, all the elements constituting the solar collector are at the ambient temperature. For the first section where j = 1, the collector temperatures are those of the ambient air. Then, for each section of the collector and for each time step , a matrix system of equations is obtained. Its resolution makes it possible to calculate the temperatures of the solar collector elements and essentially the outlet air temperature which is further taken as the inlet air temperature heating the drying chamber.

3.4.2 Determination of heat transfer coefficient for the solar collector

Heat transfer in the solar collector and in the drying chamber is carried out in three modes. Namely, heat transfer by conduction, heat transfer by convection and heat transfer by radiation. The heat transfer coefficient for these transfer modes are determined using the following equations: [19, 12].

Radiation heat exchange between glass face and sky.

$$\mathrm{hrgs} = \sigma\varepsilon_g(T_s + T_{g1})(T_s^2 + T_{g1}^2) \tag{3.40}$$

with $T_s = 0.0852.\,T_a^{1.5}$

Radiation heat exchange between first glass cover and second glass cover.

$$\mathrm{hr}_{gg} = \sigma\varepsilon_{g1}\varepsilon_{g2}\frac{(T_{g1} + T_{g2})(T_{g1}^2 + T_{g2}^2)}{\varepsilon_{g1} + \varepsilon_{g2} - \varepsilon_{g1}\varepsilon_{g2}} \tag{3.41}$$

Radiation heat exchange between second glass cover and the absorber plate.

$$\mathrm{hr}_{gp} = \sigma\varepsilon_{g2}\varepsilon_p\frac{(T_{g2} + T_p)(T_{g2}^2 + T_p^2)}{\varepsilon_{g2} + \varepsilon_p - \varepsilon_{g2}\varepsilon_p} \tag{3.42}$$

Radiation heat exchange between absorber plate and the internal face of insulation.

$$\mathrm{hr}_{pi} = \sigma\varepsilon_p\varepsilon_{ii}\frac{(T_p + T_{ii})(T_p^2 + T_{ii}^2)}{\varepsilon_p + \varepsilon_{ii} - \varepsilon_p\varepsilon_{ii}} \tag{3.43}$$

Radiation heat exchange between the external face of insulation and the sky.

$$hr_{is} = \sigma\varepsilon_g(T_{ie} + T_s)(T_{ie}^2 + T_s^2) \quad (3.44)$$

Heat exchange by convection between upper face of first glass cover.

$$hv = 5.67 + 3.88.V_{wind} \quad (3.45)$$

Heat exchange by convection between first glass cover and second cover.

$$hv_{gg} = \frac{Nu.\lambda_a}{ep} \quad (3.46)$$

Heat exchange by convection between second glass cover and absorber plate.

$$hv_{gp} = \frac{Nu.\lambda_a}{ep} \quad (3.47)$$

Heat exchange by convection across the absorber plate and internal insulation with the air flowing in this path.

$$hv_{pf} = hv_{fi} = \frac{Nu\,.\lambda air}{D_H} \quad (3.48)$$

where:

$$Nu = 0.018\,Re^{0.8}.Pr\,\hat{}0.4 \quad (3.49)$$

$$Re = (U.D_H.\rho_{air})/\mu_{air} \quad (3.50)$$

$$D_H = \frac{4.width\,.ep}{2.(width + ep)} \quad (3.51)$$

3.5 Energy Balance for Drying Chamber

Inside the drying chamber, heat transfer is the main dominant phenomena. The heat is transferred in all direction between the air and products in the trays and throughout the walls of the drying up to the ambient air and the sky as shown in Fig.3.5. The developed model is based on the following simplifying assumptions:

a. The moving fluid is considered to be in one-dimensional flow.
b. The temperatures of the various solid elements are considered uniform in the plane perpendicular to the air flow.
c. The physical properties of the product and of constituent materials of solar system are considered constant; those of air vary with temperature and humidity.

d. The radiative exchanges inside the dryer are neglected.

e. Thermal losses and pressure drops of air moving through connector's junction are neglected

f. The heat transfer by conduction between rack and product is neglected.

g. The dried product is considered as a sphere.

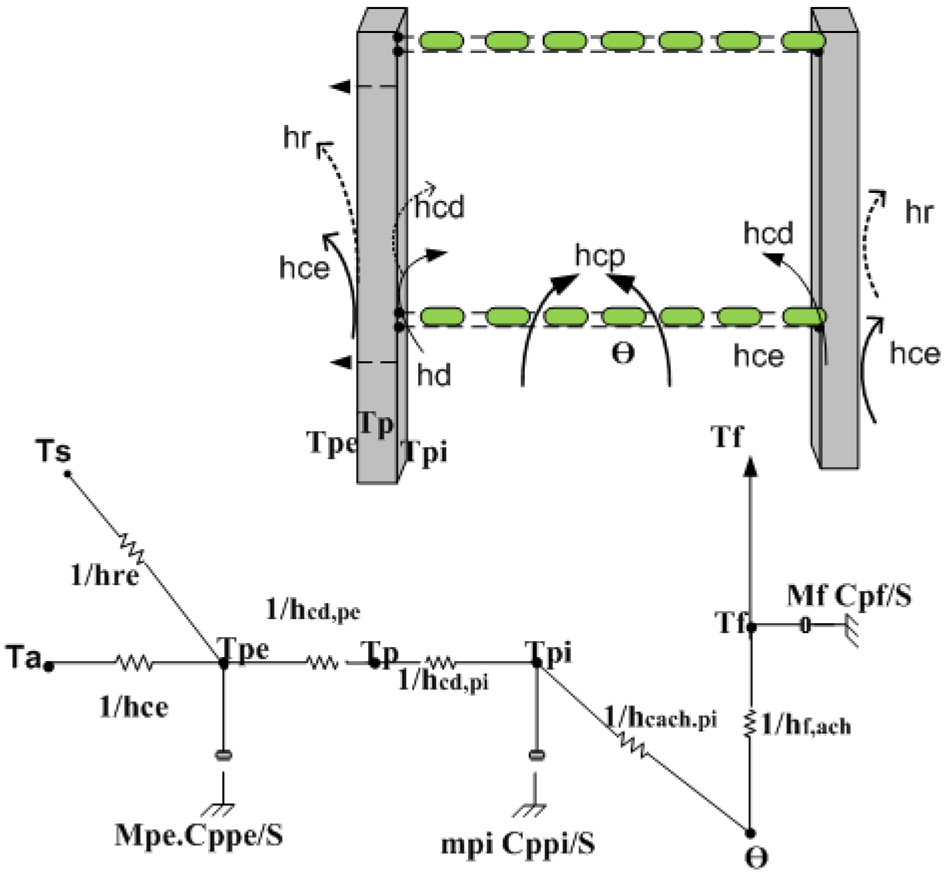

Fig. 3. 5 Thermal circuit representing heat exchange in the drying chamber

In a particular section slice referred as "j" , the analysis using the thermal circuit as shown in Fig.3.5 leads to the following equations

Through the wall:

At the external wall face

$$m_{pi}Cp_{pe}\left(\frac{dT_{pe}}{dt}\right) = h_{ce}.S_p\left(T_a - T_{pe}\right) + h_{re}.S_p\left(T_c - T_{pe}\right) + h_{cd,pe}.S_p\left(T_p - T_{pe}\right) \quad (3.52)$$

At the internal wall face

$$m_{pi}Cp_{pi}\left(\frac{dT_{pi}}{dt}\right) = h_{cd,pi}.S_p\left(T_p - T_{pi}\right) + h_{cash,pi}.S_p\left(\theta_{(j-1)} - T_{pi}\right) \quad (3.53)$$

Inside the drying chamber:

Exchange between the product, internal wall face and the drying air

$$Q.Cp\left(\theta_{(j)} - \theta_{(j-1)}\right) = h_{cash,pi}.S_p\left(T_{pi} - \theta_{(j-1)}\right) + h_{cf,cash}.S\left(T_f - \theta_{(j-1)}\right) \quad (3.54)$$

Exchange between the product and the drying air

$$m_{pi}Cp_{pe}\left(\frac{dT_{pe}}{dt}\right) = h_{cf,ach}.S\left(\theta_{(j-1)} - T_f\right) - P_{ev} \quad (3.55)$$

Exchange through the wall between internal and external faces)

$$m_{pe}Cp_{pe}\left(\frac{dT_p}{dt}\right) = h_{cd,pe}.S_p\left(T_p - T_e\right) = m_{pi}Cp_{pi}\left(\frac{dT_p}{dt}\right) = h_{cd,pi}.S_p\left(T_{pi} - T_p\right) \quad (3.56)$$

Next these equations are discretized for the numerical study as follow:

At the external wall face

$$m_{pe}Cp_{pe}\left(\frac{T_{pe}^{t+\Delta t}(j) - T_{pe}^{t}(j)}{\Delta t}\right) = h_{ce}.S_p\left(T_a - T_{pe}^{t+\Delta t}(j)\right) + h_{re}.S_p\left(T_c - T_{pe}^{t+\Delta t}(j)\right) + h_{cd.pe}.S_p\left(T_p^{t+\Delta t}(j)\right) - T_{pe}^{t+\Delta t}(j)) \quad (3.57)$$

At the internal wall face

$$m_{pi}.\,Cp\left(\frac{T_{pe}^{t+\Delta t}(j)-T_{pe}^{t}(j)}{\Delta t}\right)$$
$$=h_{cd,pi}.\,S_p\left(T_p^{t+\Delta t}(j)-T_{pi}^{t+\Delta t}(j)\right)\qquad(3.58)$$
$$+h_{cash}.\,S_p\left(\theta^{t+\Delta t}(j-1)-T_{pi}^{t+\Delta t}(j)\right)$$

Inside the drying chamber

Exchange between the product, internal wall face and the drying air

$$Q.\,Cp\left(\theta^{t+\Delta t}(j)-\theta^{t+\Delta t}(j-1)\right)$$
$$=h_{cf,ach}.\,S_p\left(T_{pi}^{t=\Delta t}(j)-\theta^{t+\Delta dt}(j-1)\right)\qquad(3.59)$$
$$+h_{cf,ach}.\,S(T_f^{t+\Delta t}(j)-\theta^{t+\Delta t}(j-1))$$

Exchange between the product and the drying air

$$m_fCp_f\left(\frac{T_f^{t+\Delta t}(j)-T_p^{t}(j)}{\Delta t}\right)\qquad(3.60)$$
$$+h_{cf,ach}.\,S_p\left(\theta^{t+\Delta t}(j-1)-T_f^{t+\Delta t}(j)\right)-P_{ev}$$

Exchange through the wall between internal and external faces)

$$m_{pe}Cp_{pe}\left(\frac{T_f^{t+\Delta t}(j)-T_p^{t}(j)}{\Delta t}\right)+h_{cd,pe}.\,S_p\left(T_p^{t+\Delta t}(j)-T_{pe}^{t+\Delta t}(j)\right)$$
$$=m_{pi}Cp_{pi}\left(\frac{T_p^{t+\Delta t}(j)-T_p^{t}(j)}{\Delta t}\right)\qquad(3.61)$$
$$+h_{cd,pi}.\,S_p\left(T_{pi}^{t+\Delta t}(j)-T_p^{t+\Delta t}(j)\right)$$

where:

$$S_p=2.\,(\text{width}+\text{depth}).\,\Delta x\qquad(3.62)$$

Δx: length of the section

By putting all these equations together, we get a system of five equations with five unknowns which are: $T_{pe}, T_p, T_{pi}, T_f, \theta$ which can be solved using a matrix form as follow:

$$\begin{bmatrix} A_{11} & A_{21} & A_{31} & A_{41} & A_{51} \\ A_{12} & A_{22} & A_{32} & A_{42} & A_{52} \\ A_{13} & A_{23} & A_{33} & A_{43} & A_{53} \\ A_{14} & A_{24} & A_{34} & A_{44} & A_{56} \\ A_{15} & A_{25} & A_{35} & A_{45} & A_{55} \end{bmatrix} . \begin{bmatrix} T_f^{t+\Delta t}(j) \\ \theta^{t+\Delta t}(j) \\ T_{pi}^{t+\Delta t}(j) \\ T_p^{t+\Delta t}(j) \\ T_{pe}^{t+\Delta t}(j) \end{bmatrix} = \begin{bmatrix} B_1 \\ B_2 \\ B_3 \\ B_4 \\ B_5 \end{bmatrix} \tag{3.63}$$

Whereas the matrix entries are:

$$A_{11} = \frac{m_f . Cp_f}{\Delta t} + S . h_{cf,ach} \tag{3.64}$$

$$B_1 = \frac{m_f . Cp_f}{\Delta t} T_f^t(j) + h_{cf,ach} . S . \theta^{t+\Delta t}(j-1) - P_{ev} \tag{3.65}$$

$$A_{21} = -s . h_{cf,ach} \tag{3.66}$$

$$A_{12} = Q . Cp \tag{3.67}$$

$$A_{23} = -S_p . h_{cach,pi} \tag{3.68}$$

$$\begin{aligned} B_2 = Q . Cp . \theta^{t+\Delta t}(j-1) - S_p . h_{cach,pi} . \theta^{t+\Delta t}(j-1) \\ - S . h_{cf,ach} . \theta^{t+\Delta t}(j-1) \end{aligned} \tag{3.69}$$

$$A_{33} = \left(m_{pi} . \frac{Cp_{pi}}{\Delta t}\right) + h_{cd,pi} . Sp + h_{cach,pi} . Sp \tag{3.70}$$

$$A_{34} = -S_p . h_{cd,pi} \tag{3.71}$$

$$B_3 = \left(m_{pi} . \frac{Cp_{pi}}{\Delta t}\right) T_{pi}^t + h_{cach,pi} . Sp . \theta^{t+\Delta t}(j-1) \tag{3.72}$$

$$A_{34} = -h_{cd,pi} . Sp \tag{3.73}$$

$$A_{44} = \left(\frac{m_{pe} . Cp_{pe} - m_{pi} . Cp_{pi}}{\Delta t}\right) + h_{cdpe} . S_p + h_{cd,pi} . Sp \tag{3.74}$$

$$A_{45} = -h_{cd,pe} . Sp \tag{3.75}$$

$$B_4 = \left(\frac{m_{pe} . Cp_{pe} - m_{pi} . Cp_{pi}}{\Delta t}\right) T_p^t(j) \tag{3.76}$$

$$A_{54} = -h_{cd,pe} . Sp \tag{3.77}$$

$$A_{55} = \left(m_{pe} . \frac{Cp_{pe}}{\Delta t}\right) + h_{ce} . S_p + h_{re} . Sp + h_{cdpe} . Sp \tag{3.78}$$

$$B_5 = \left(m_{pe} . \frac{Cp_{pe}}{\Delta t}\right) T_{pe}^t + h_{ce} . Sp . Ta + h_{cd,pe} . Sp . Tc \tag{3.79}$$

3.5.1 Simulation flowchart for the drying chamber

The simulation flowchart for the drying chamber program is shown in Fig. 3.6. At the staring time, all the dryer constituents and of the green paper product are at the ambient temperature. For the first tray of the dryer (j = 1), the temperature of the dryer is that of solar collector air output for a system without backup system. For this system, this values depends on the solar intensity and ambient temperature. In the case a backup system is used, the temperature of the first tray are mainly assumed constant from morning up tonight. In the next step of flowchart, for each tray and for each step of time, a system of equations is obtained. Its resolution makes it possible to calculate the temperatures different components of the dryer, the temperature of the product to be dried and that of the drying air. Note that in the establishment of systems of equation drying kinetics of the product is considered. The used kinetic model is taken from experimental work. Regarding the transfer coefficients, their calculation is carried out for each time step and for each slice. For solving the system of equations, the Gauss Seidel method is used.

<u>Flowchart for the drying chamber simulation program</u>

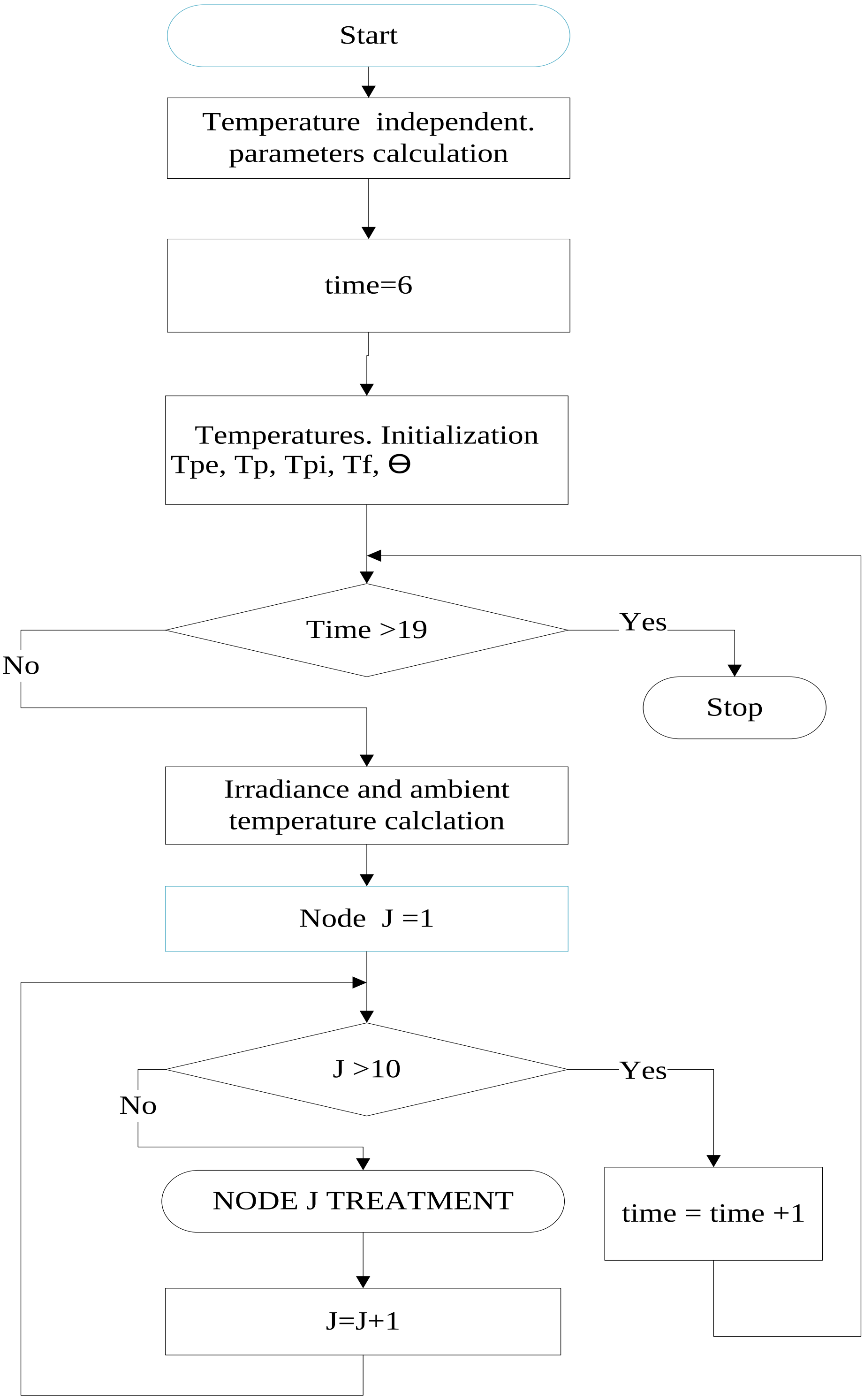

Fig. 3. 6 Simulation flowchart for the drying chamber program

Flowchart for nodes J treatment

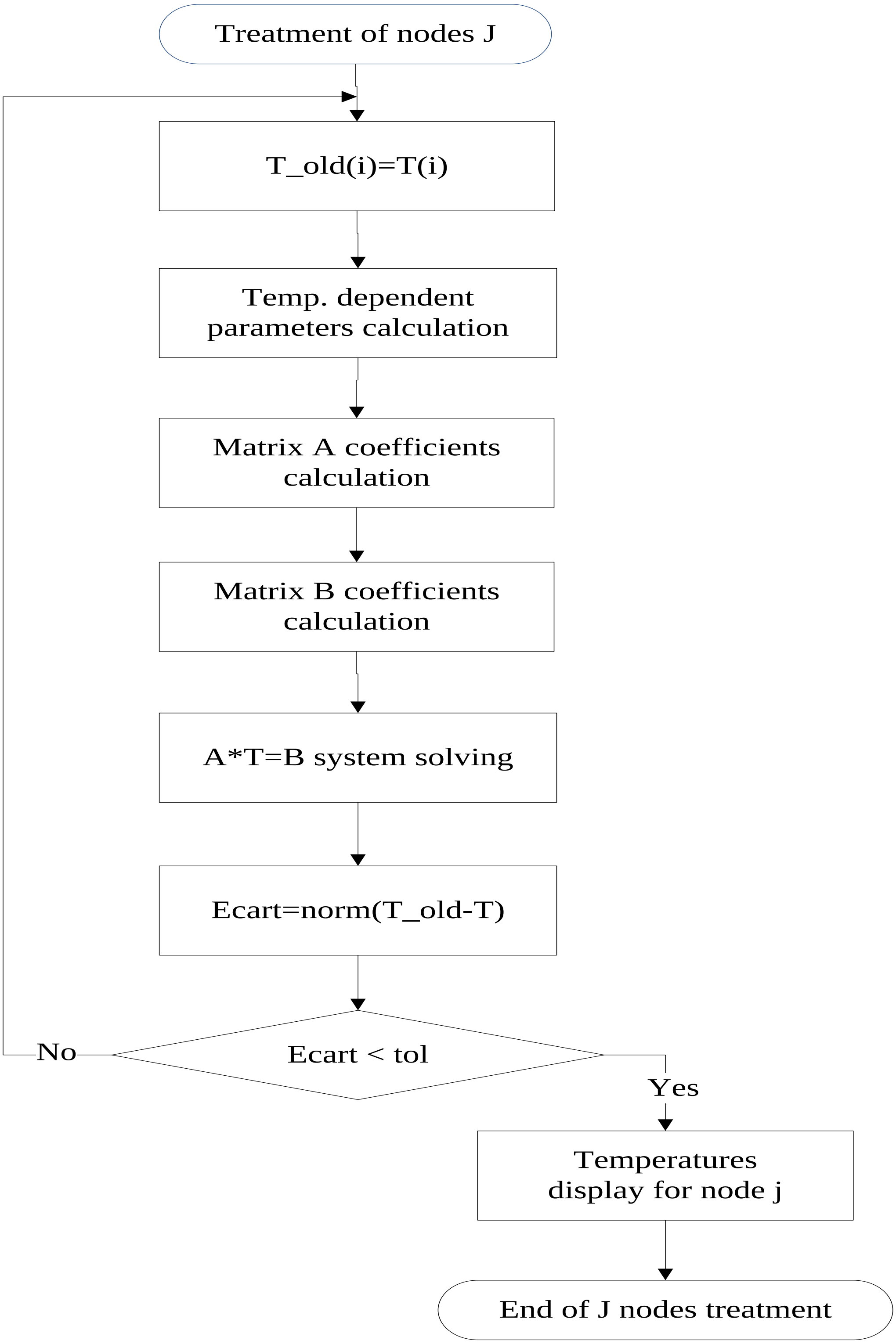

Fig. 3. 7 Flowchart for nodes J treatment in the drying chamber program

3.5.2 Determination of heat transfer coefficient for the drying chamber

Heat transfer for drying chamber by convection between ambient air and external wall of drying chamber.

$$h_{ce} = 5.67 + 3.86\, V_{wind} \tag{3.80}$$

Heat transfer by convection between the internal wall of drying chamber and the drying air.

$$h_{cach,pi} = Nu_{pi} \cdot \frac{\lambda_{air}}{D_H} \tag{3.81}$$

D_H: The hydraulic diameter defined as:

$$D_H = \frac{4.\,S}{2.\,(larg + prof)} \tag{3.82}$$

$$Nu_{pi} = 0.023.\, Re_{pi}^{0.8}.\, P_r^{0.33} \tag{3.83}$$

$$Re_{pi} = U.\, D_H \cdot \frac{\rho_{ah}}{\mu_{ach}} \tag{3.84}$$

$$Pr = \frac{\mu_{air}\,.\, Cp_{air}}{\lambda_{air}} \tag{3.85}$$

with:

ρ_{ah} = hot air density (kg/m^3)

μ_{air} = dynamic viscosity $(kg/m.\, s\,)$

Cp_{air} = specific heat of air $(W/kg.\, K)$

λ_{air} = coefficient of thermal conductivity for air $(W/m.\, K)$

U = mean speed of moving fluid.

Heat transfer by convection between the drying air and surface product.

$$h_{cach,f} = \frac{Nu_D\,.\, \lambda_{air}}{D_f} \tag{3.86}$$

where:

$$Nu_D = 2 + 0.03.\, P_r^{0.33}.\, Re_D^{0.54} + 0.35\,.\, P_r^{0.36}.\, Re_D^{0.58} \tag{3.87}$$

$$Re_D = \frac{U_f\,.\, D_f\,.\, \rho_{ah}}{\mu_{ah}} \tag{3.88}$$

U_f = air velocity around the product calculated as follow

$$U_f = \frac{U}{P_o} \quad (3.89)$$

With U being the air velocity inside the dryer as seen above whereas P_0 is the porosity rate. It is equal to:

$$P_o = 1 - OC \quad (3.90)$$

OC = occupation rate

where:

$$OC = n\frac{\pi D_f^3}{6}\frac{1}{long\,.\,larg.\,D_f} \quad (3.91)$$

with:

n = number of the dried product put on each tray,

long = length (m),

larg = width (m),

D_f = product diameter.

3.5.3 Evaporative power during water phase changing

Evaporative power is the power lost by dried product due to its water phase changing. It is given by the following formula [14]:

$$P_{ev} = m_{sec}\,.\,L_v\,.\frac{dX}{dt} \quad (3.92)$$

with:

L_v = latent heat of vaporization (J/kg)

where:

$$L_v = 4186.8\,(597 - 0.56T_f) \quad (3.93)$$

with:

m_{sec} = dry product mass (kg)

3.5.4 Mass transfer in air

The variation of air humidity is calculated using the following expression:

$$\left(W_{ach,0} - W_{ach}\right)\dot{m}_{ach} = K(X - X_e)m_{sec} \quad (3.94)$$

Where $W_{ach,0}$ is the absolute humidity of the air stream passing through the solids phase (kg/kg db), W_{ach} is the absolute humidity of this stream on leaving the solids (kg/dg db), $\dot{m}_{ach}$ is the stream's mass flowrate, and m_{sec} is the total dry mass of the solid phase [17]. The variation of product moisture content X during the drying time is calculated by using kinetic drying models.

3.5.5 Drying rate calculation

The moisture transfer during drying can be described using a first-order kinetic model as mentioned below:

$$\frac{dX}{dt} = -K(X - Xe) \qquad (3.95)$$

With X being the product moisture content expressed in dry basis and X_e is the equilibrium moisture content of dried products and t taken as time.

Taking the moisture content $X = X_i$ at t=0 the solution is found for the moisture content at any time as in the following expression [6]:

$$\frac{X_t - X_e}{X_i - X_e} = e^{-Kt} \qquad (3.96)$$

The relationship for the equilibrium moisture content for green pepper Xe is found in [7].

The drying constant K insures the falling rate slope of drying curve. It is a function of the material characteristic dimension and drying condition determined by [18]:

$$K = K_0 D_f^{KD} T_{ach}^{KT} W_{ach}^{KW} U_{ach}^{KU} \qquad (3.97)$$

with:

D_f = characteristic dimension taken as equal to 5 cm,

W_{ach} = absolute humidity of air stream taken as equal to 0.022 kg/kg,

U_{ach} = velocity of drying air mainly taken as 2 m/s.

T_{ach} = Temperature of drying air.

where:

$K_0 = 2.77778 \times 10^{-6}\ (s^{-1})$

$KD = -0.92$

$\mathrm{KT} \quad = 1.5$

$\mathrm{KW} \quad = 0.09$

$\mathrm{KU} \quad = -0.29$

K_o, KD, KT, KW, KU are empirical constants changing from product to another,

The corresponding constants from the dried product (green pepper) are found in the experiment carried out by Kiranoudis et al [18]. Note that the value of K_0 are transformed from the units of hours to the seconds.

3.5.6 Determination of specific of dried product

The Specific heat Cp_fcharacterizing the quantity of heat gained or lost by a unit mass of product to accomplish a unit change in temperature, without a change in state. During the thermal analysis of food processing and in designing drying equipment, we need numerical values for the specific heat of the food. Choi and Okos (1986) presented a predictive model to predict specific heat based on composition and temperature. Their model is as follows [15]:

$$Cp_f = \sum_{i=1}^{n} C_{pi} x_i \tag{3.98}$$

where, x_i is the fraction of the any particular component, n is the total number of components in a food, and C_{pi} is the specifi c heat of the i^{th} component.

3.6 Estimation of Input Data

3.6.1 Calculation of Solar Time

The solar radiation intensity at a given location depends on the sun position in the sky. In turn, the sun position varies with time as the earth rotates and revolves around the sun. To know the orientation of the sun at a given location requires first the location position on earth and the related sun position angles. The site location is firstly characterized by the Earth horizontal divisions called latitude representing the angle between the center of the earth to the site and the equatorial plane. Secondly by the longitudinal divisions known as longitudes describing how many degrees the site lie to the east or west of the prime meridian. Kigali –Rwanda,is located at the latitude is -1.935 and the longitude is 30.082°. These values can be determined by the use of atlas or other online means.

On the other hand, the solar position as the sun moves depends on time. In solar work typically apparent solar time is used and obtained from the local standard time observed on a clock by making two corrections as shown in the next equation. The first correction is due to difference in longitude between the location and the meridian on which the standard time is based. The second correction is due to the equation of time. The factor of 4 in the equation is due to the fact that it takes 4 mins to move each degree of longitude [10].

$$\mathrm{AST} = \mathrm{LST} + \frac{4}{\mathrm{deg}}(\mathrm{Long} - \mathrm{LSTM}) + \mathrm{ET} \tag{3.99}$$

with:

LST = local clock time

Long = local longitude

STM = local longitude of standard time meridian

ET = equation of time

where:

$$\mathrm{LSTM} = 15^0\left(\frac{\mathrm{Long}}{15^0}\right)_{\text{rounded to integer}} \tag{3.100}$$

$$\mathrm{ET} = 9.87 * \sin(2 * \mathrm{D}) - 7.53 * \cos(\mathrm{D}) - 1.5 * \sin(\mathrm{D}) \tag{3.101}$$

With D standing for longitude correction for a day number n obtained in degrees as

$$\mathrm{D} = 360 * (\mathrm{n} - 81)/365 \tag{3.102}$$

3.6.2 Solar angles Determination

The sun angles are obtained from the calculated local solar time. The important angle characterizing the position of the sun include azimuth and altitude angles but they are not fundamental angles [10]. They are found by using latitude angles, declination and hour angle. The declination is the angle linking the lines joining the center of the earth to the sun with its projection on the equator plane. It denotes the tilt of the Earth’s axis and rotation around the sun that causes variation in the angle at which the sun rays strikes a surface at the Earth. It is given in degrees as

$$\delta = 23.45 * \sin\left(\frac{360}{365} * (284 + n)\right) \quad (3.103)$$

with:

δ = declination

n = day number of the year

The solar altitude β1 also called solar elevation is the angle between the horizon and the center of sun. It represents the apparent height of the sun relative to the panels. Its value and the value of complement zenith angle θz are given by:

$$\sin(\beta_1) = \cos(\theta_z) = \sin(\delta) * \mathrm{Sin}(\Phi) + \mathrm{Cos}(\delta) * \mathrm{Cos}(\Phi) * \mathrm{Cos}(H) \quad (3.104)$$

with:

β_1 = solar altitude

θ_z = zenith angle

Φ = Latitude

H = hour angle

Where the Hour angle H is the azimuth angle of the sun's rays caused by the earth's rotation calculated as:

$$H = \frac{\text{local time in minutes } - 720}{4} \quad (3.105)$$

The altitude angle at the time of sunrise and sunset is 0^0, the hour angle at sunset and sunrise is determined by:

$$\mathrm{Cos}(Hs) = -\tan(\Phi) * \tan(\delta) \quad (3.106)$$

The sunrise hour angle and sunset hour angle are four by:

$$H_{sr} = -\mathrm{Cos}^{-1}[-\tan(\Phi) * \tan(\delta)] \quad (3.107)$$

$$H_{ss} = \mathrm{Cos}^{-1}[-\tan(\Phi) * \tan(\delta)] \quad (3.108)$$

with:

H_{sr} = hour angle at sunrise

Hss = hour angle at sunset

The number of sunshine hours per day is obtained by:

$$N = \frac{2}{15}\mathrm{Cos}^{-1}(-\tan(\Phi) * \tan(\delta)) \quad (3.109)$$

The azimuth angle which is the angle in the horizontal plane measured from true north to the horizontal projection of the sun's rays was found by:

$$\alpha_1 = \mathrm{acos}\left(\frac{\sin(\beta_1) * \sin(\Phi) - \sin(\delta)}{\cos(\beta_1) * \mathrm{COS}(\Phi)}\right) \quad (3.110)$$

with:

α_1 = azimuth angle

Its value is positive in the afternoon and negative in the morning as its sign is matched by the hour angle sign. Azimuth measures the sun's angle relative to north, in the eastward or westward directions. If the sun is due north in the sky, the azimuth will be zero. If the sun is due east in the sky, the azimuth angle will be minus 90 degrees. Using the above formulae, the exact position of the sun could be tracked daily by using the obtained solar altitude and solar azimuth angles at different times of the day. The solar air heater :array angle (θ) between the sun and normal to its surface is given by

$$\cos(\theta) = \sin(\beta_1) * \cos(\beta_2) + \mathrm{co}(\beta_1)\sin(\beta_2)\cos(\alpha_1 - \alpha_2) \quad (3.111)$$

with:

β_2 = tilt angle of solar collector

α_2 = azimuth angle solar collector

The calculated different angles values appears on the excel sheet given the name of month. Their results are given hourly and correspond to the input given at solar time sheet. Notice that in solar design it is important to remember that when evaluating a solar collector located in the southern hemisphere, north is always used as the reference direction and is marked zero. The orientation is expressed as the number of degrees east or west of true north. For example, $\alpha_2 = 25$ degrees east of true north. Also it is noted that true north is different from magnetic north because of the phenomenon of declination.

3.6.3 Estimation of Solar Radiation Intensity

Solar radiation incident on the atmosphere from the direction of the sun is called extraterrestrial solar beam radiation. Its intensity is approximated by [9]:

$$\mathrm{I} = \mathrm{I_0}\left(1 + 0.034\cos\left(\frac{360\ \mathrm{n}}{365.25}\right)\right) \quad (3.112)$$

As it passes through the earth's atmosphere it is attenuated and scattered. Beneath the atmosphere, at the Earth's surface, the radiation that is observed include the direct beam radiation ($\mathrm{I_{b,N}}$) and the solar radiation received from the sun having been scattered by the atmosphere referred as diffuse radiation ($\mathrm{I_{d,h}}$). According to the ASHRAE model these two components are calculated as [10]:

$$\mathrm{I_{b,N}} = \mathrm{Ie}^{-\tau_b m^b} \quad (3.113)$$

$$\mathrm{I_{d,N}} = \mathrm{Ie}^{-\tau_d m^b} \quad (3.114)$$

with:

$\mathrm{I_{b,N}}$ = direct beam radiation,

$\mathrm{I_{d,h}}$ = diffuse radiation,

m = air mass ratio,

τb = beam optical depths,

τd = diffuse optical depths,

b = beam air mass exponent,

d = diffuse air mass exponent.

where:

$$\mathrm{m} = \frac{1}{\sin(\beta_1) + 0.50572(6.07995 + (\beta_1))^{-1.6364}} \quad (3.115)$$

The values of τ_b and τ_d are location specific obtained for each day by the interpolation of their average values tabulated for 21st day of each month for all the locations in the tables of climatic design conditions in the tables of climatic design condition. The values of b and d are obtained from the following empirical relationships [10]:

$$\mathrm{b} = 1.219 - 0.043\tau_b - 0.151\tau_d - 0.204\tau_b\tau_d \quad (3.116)$$

$$\mathrm{d} = 0.202 + 0.852 - 0.007\ \tau_d - 0.357\tau_b\tau_d \quad (3.117)$$

The total solar radiation on a horizontal surface is given by

$$I_h = I_{b,N}\sin(\beta_1) + I_{d,h} \quad (3.118)$$

with:

I_h = total solar radiation on a horizontal surface

The total solar radiation on a tilted solar collector is the sum of the collector beam $I_{b,c}$, the diffuse $I_{d,c}$ and reflected $I_{r,c}$ solar radiation as:

$$I_c = I_{b,c} + I_{d,c} + I_{r,c} \quad (3.119)$$

with:

I_c = total solar radiation on a tilted solar collector

$I_{b,c}$ = collector beam

$I_{d,c}$ = diffuse beam

$I_{r,c}$ = reflected beam

Given that the angle of incidence of the beam radiation on the array surface, then

$$I_{b,c} = I_{b,N}\cos\theta \quad (3.120)$$

The diffuse radiation on the surface is obtained by multiplying the sky diffuse radiation on a horizontal surface by the view factor between the sky and the surface

$$I_{d,c} = I_{d,h}\cos^2(\frac{\beta_2}{2}) \quad (3.121)$$

The part intercepted of the ground reflected solar radiation intercepted by is found from the total solar radiation incident on a horizontal surface and the ground reflectance ρ multiplied by the view factor equaling to:

$$I_{r,c} = \rho I_h \sin^2(\frac{\beta_2}{2}) \quad (3.122)$$

The calculated values for solar irradiance components also appears on the excel sheet called month. Their results are given hourly and correspond to the input to the solar air.

This Page Is Intentionally Left Blank

CHAPTER 4
RESULTS AND DISCUSSION

The principle behind the design of an indirect solar dryer is related to the relative and absolute humidity of air. Air can suck moisture vapor from product but only up to a certain limit. This limit is called absolute maximum humidity. When air passes over wet food, it will suck its moisture until it is virtually fully saturated. At this point, the absolute humidity has reached its maximum. But interestingly, the capacity of the air for removing moisture dependends on its temperature. The higher the temperature, the higher the absolute humidity is and the larger the uptake of moisture will be. When the temperature of air raises, the amount of moisture in it stays constant but the relative humidity will fall down. With this reduction in relative humidity, the air is enabled to take up more moisture from its surrounding. The main contribution of a solar collector in an indirect solar dryer is its capacity to generate hot air using the solar radiation as result of which its moisture fixing capacity is increased. In case where the weather conditions are not friendly, a heating system can be used to heat the air entering the drying chamber. In the simulation of our solar dryer, the effects of using a solar collector with and without heating backup system are all studied. Noting that this solar dryer is designed for vegetables and fruits sellers in local markets for the purpose of drying the excess or non-sold out products. Therefore, even though an indirect solar dryer is sun dependent, the use of heating backup system will make it more practical and efficient in the time of bad weather conditions.

4.1 Input data

4.1.1 Ambient temperatures

Ambient temperature is one of the most influential parameters on the drying process. For a solar dryer using a solar collector, temperature values of the air entering for the first time into the collector are equal to the ambient temperature. A cool air will require more energy to be raised at the drying temperature of interest whereas warm air needs less energy. The theoretical variations in ambient temperature considered in this study are shown in Fig.4.1. These values are estimated by assuming that on the considered day of 21st August, the lowest temperature value during the day is 22 and the highest is 28^{0}C. This range corresponds to minimum and maximum ambient temperatures observed in Rwanda in the month of August. The theoretical model used in this estimation is similar to the method used in [19]. The model assumes that the ambient temperature is influenced by solar radiation intensity. This is based on the idea that during night, the ambient air cools down as there is no solar radiation whereas during the day it is heated up again. Such a dependency will be well illustrated after in Fig.4.3.

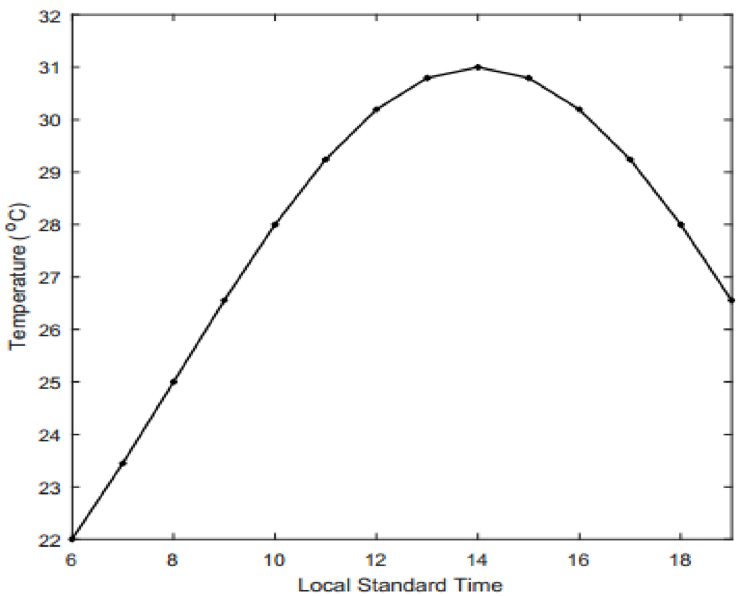

Fig. 4. 1 Ambient temperatures estimated theoretically

4.1.2 Site location and sun position angles

The behavior of an indirect solar thermal system depends greatly on the weather data, mainly on the solar radiation intensity and ambient temperature. The solar radiation intensity reaching the system depends on the sun position in the sky and on the site location. The sun position varies with time as the earth rotates and revolves around it. The location site, sun position angles as well as the related day time are vital in determination of radiation intensity captured by an installed solar collector. The mathematical model used for the estimation of solar angles is solved for Kigali-Rwanda on August 21st since this is the harvesting time for green paper. The Kigali site location is firstly characterized by the Earth horizontal divisions called latitude. The latitude at this site is equal to -1.935° characterizing the angle between the center of the earth to the site and the equatorial plane. Secondly, this site is also described by the longitudinal division known as longitude having a value of 30.082° describing how many degrees Kigali lie to the east or west of the prime meridian.

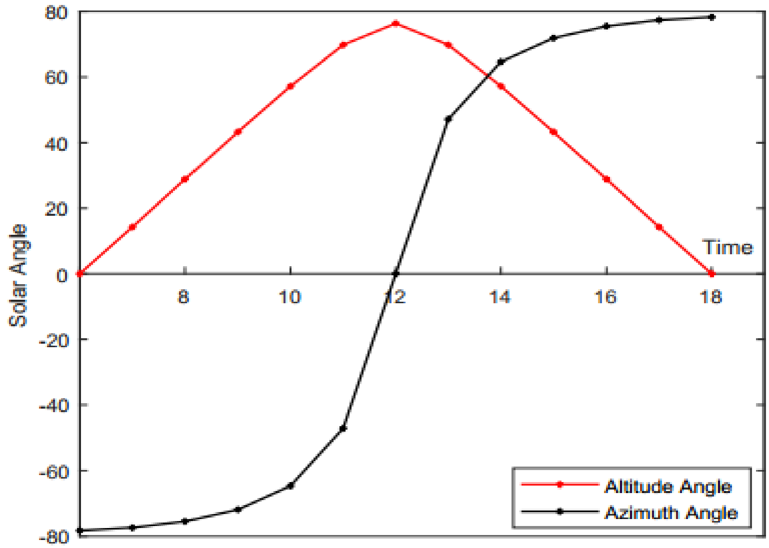

Fig. 4. 2 Altitude and azimuth angles characterizing the sun position

The important angles characterizing the position of the sun are azimuth and altitude angles. Their values used to track the exact position of the sun on August twenty first are shown in Fig.4.1 at different times of the day. These values are found by using latitude angles, declination and hour angle as seen before chapter III. It is denoted that the altitude angle at the time of sunrise and sunset is 0^0 and its maximum value is at twelve o' clock. The azimuth angle which is the angle in the horizontal plane measured from true north to the horizontal projection of the sun's rays is shown in black curve. This angle measures the sun's angle relative to north in the eastward or westward directions. It is positive in the afternoon and negative in the morning. If the sun is due to north in the sky, the azimuth will be zero. If the sun is due to east or west in the sky, the azimuth angle will be respectively -90 and +90°. The optimum position of the sun for maximum solar radiation is obtained when the sun is high in the sky and facing north. At this time the solar altitude is maximum and the solar azimuth angle is zero showing that the sun is due to north. Similar trends in the solar altitude and solar azimuth curves are observed in [20].

4.1.3 Solar Radiation Intensity variation

The results of total radiation intensity as well as its direct component for a solar collector installed at Kigali oriented north and tilted at an angle of 15^0 are showed in Fig.4.3. The distribution in total radiation reaches a theoretical maximum value of 1019 W / m² around 12:00pm . The incident direct radiation increases gradually from sunset time until reaching the maximum value from 893 W / m² at 12:00 pm and then decreases to a value close to zero at the time of sunset.

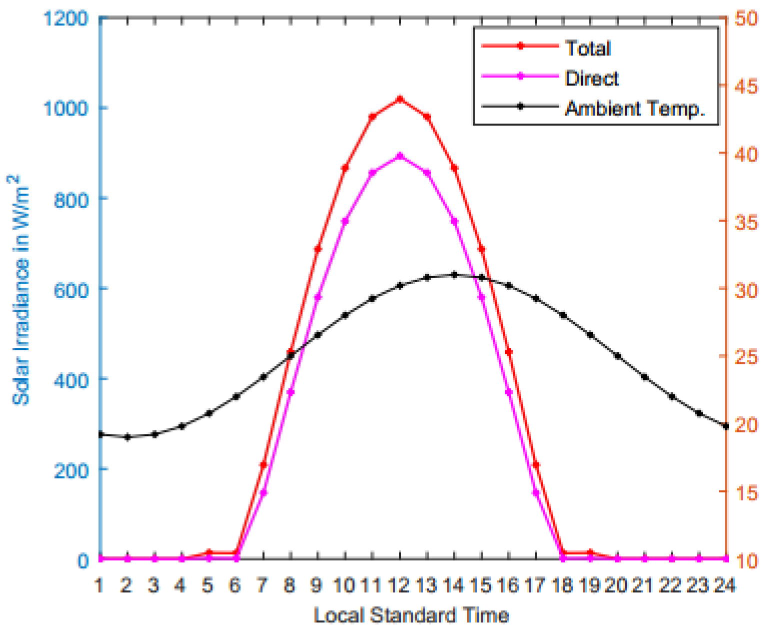

Fig. 4. 3 Diurnal variation of average hourly ambient temperature and solar intensity on captured by a solar collector on 21st August.

The diffused solar radiation component at this time had maximum value of 122 W / m² whereas the refracted radiation components is seen almost close to zero at this solar collector position. The ambient temperatures shown in black curves are shown depending on solar radiation reaching the Earth. This clearly justify that low ambient temperatures are observed during night time when there is no solar radiation while maximum values are observed in afternoon. It is noted that the maximum total solar radiation intensity occurs at 12:00 pm whereas the maximum ambient temperature value lies three hours after at 3:00 pm. This difference in the time of maximum solar radiation and maximum ambient temperature is based on the fact that warming up the surrounding air and environments takes time. Similar findings in curves trends were obtained and justified by previous research [11].

4.1.4 Influence of solar collector angle on the solar radiation components

The total flux per unit area for the inclined solar collector is the sum of three components. The investigation in the variation of collector inclination and orientation angle showed that differences from the direct component, the diffused and reflected components are greatly influenced by the inclination angle compared to orientation angle. The direct beam component which is the solar irradiance that reaches the collector directly from the sun's apparent position in the sky. It has been noted that the influence of collector inclination angle between 0^0 and 30^0 degrees does not change much the direct solar component on the considered day but for higher tilt angle it decreases considerably. This might be explained by the fact that the site is nearby the equator. The investigation in the variation of this component based on the variation of collector orientation is shown in figure Fig. 4.4, On the other hand, the effect of collector orientation on the direct solar flux was seen to be more influential. Fig.4.4. shows that orienting the solar collector south led to very low value due to the fact that some direct sunlight rays miss the collector as the sun is located on the northern side. Orientation to the east or west direction led to low values of direct radiation component as the sunset or sunrise may occur early or late.

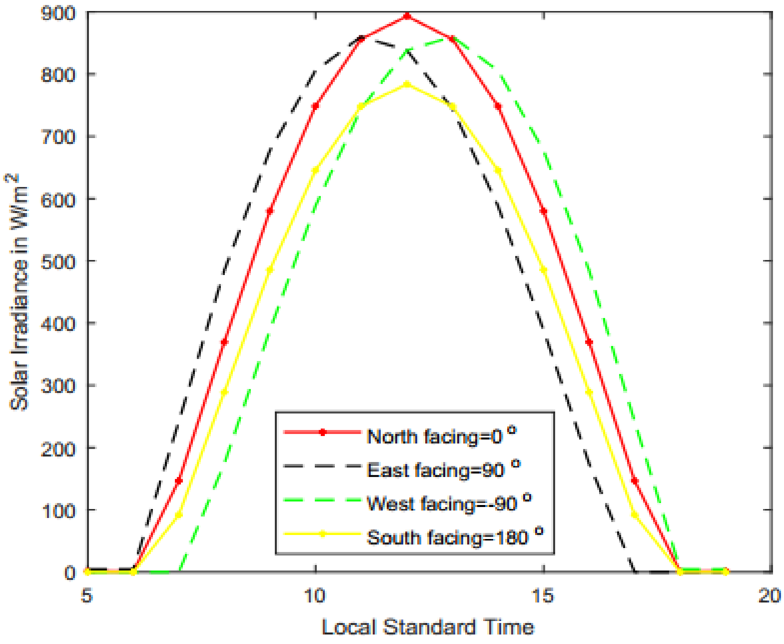

Fig. 4. 4 Influence of orientation angle variation on the direct solar radiation

There is also a diffuse component that comes from other parts of the sky after multiple scattering from sky molecules such dust particles and water molecules in clouds. On an overcast day the diffuse component dominates the direct beam, but it can be considerable even on a clear day. Fig. 4.5 shows that the increase in diffused angle is inversely proportional to the increase in tilt angle. The change in hourly values of this diffused radiation component are seen not to vary much between 0^0 and 20^0 degrees of tilt angle. This is might be due to the fact that radiation diffused from sky cloud does not reach fully a highly inclined solar collector. It is noted that the orientation angle does not have much effect on the reflected solar components as it is the irradiance reflected by the ground. On the other hand, it is noted in Fig.4.6 that low values of solar collector inclination angle lead to very low values of reflected radiation component. This is supported by the fact that an inclined solar collector surface captures much radiation reflected from the ground whereas a horizontal surface practically does not capture any radiation from the ground.

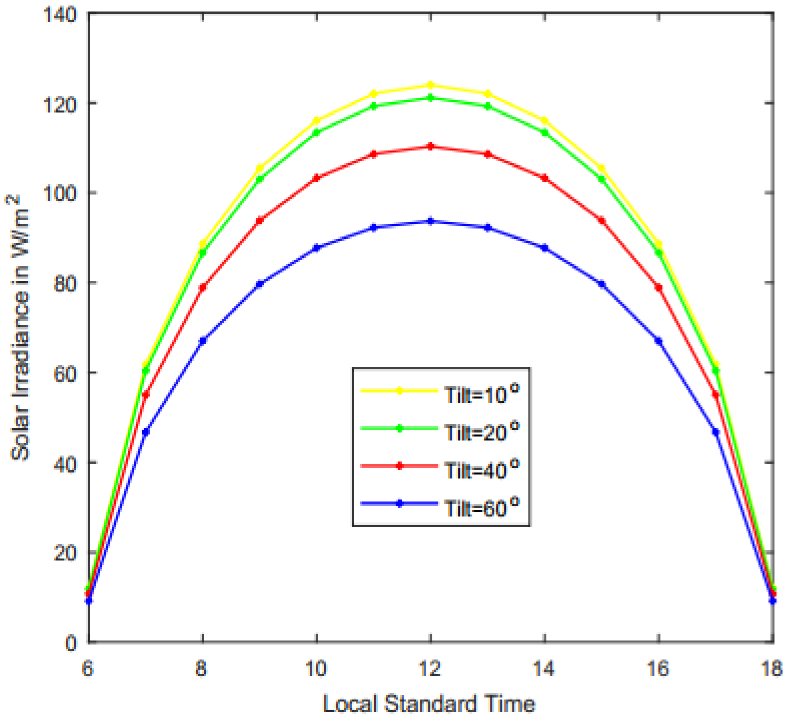

Fig. 4. 5 Influence of inclination angle variation on the diffused solar radiation

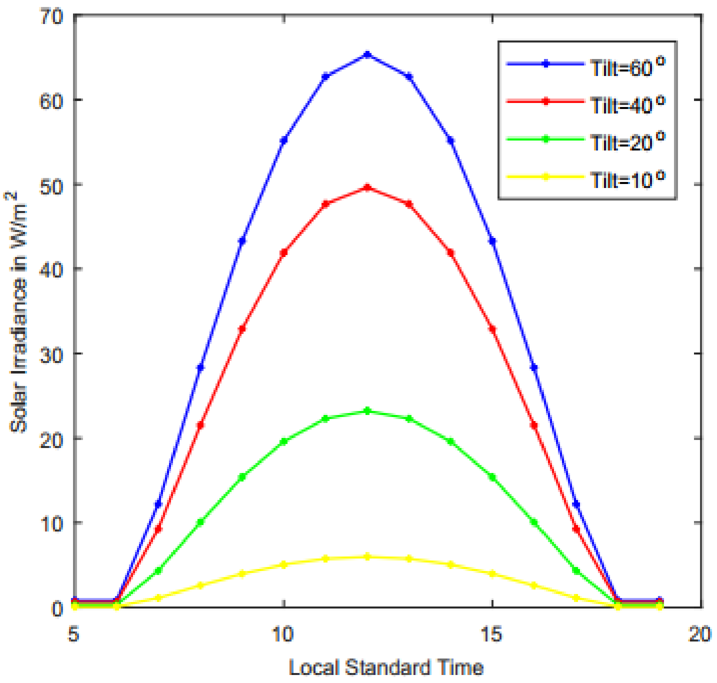

Fig. 4. 6 Influence of inclination angle variation on the reflected solar radiation

4.2 Simulation results of the solar collector

A simulation program is a multipurpose tool to use in various studies. The developed Matlab program for the solar collector fits perfectly in studying the behaviors of double glazed solar air heater. Figure 4.7 indicates hourly temperatures for various solar collector elements as well as output air fluid temperatures.

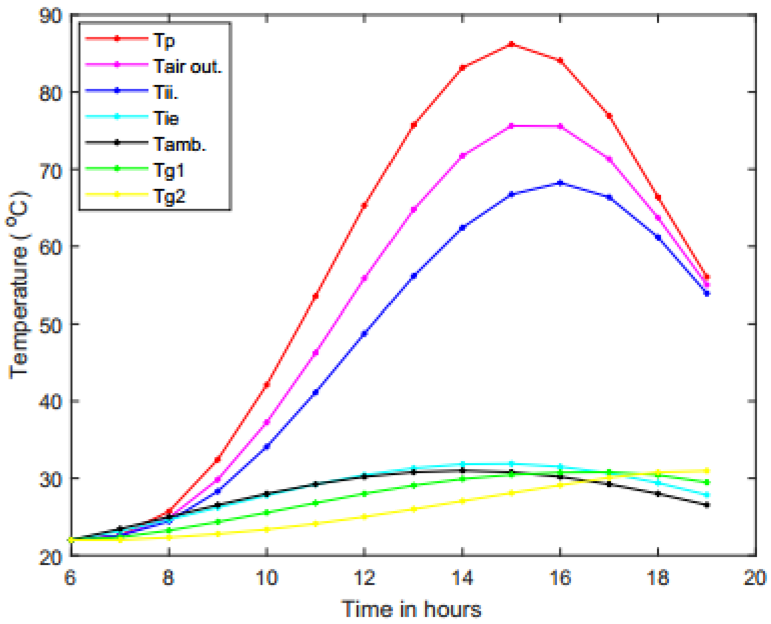

Fig. 4. 7 Variation in temperatures for different solar collector components

where:

T_P:	Temperature of the absorber plate
Tf_{out}:	Temperature of the output air fluid
T_{ii}:	Temperature of the internal face of insulation
T_{ie}:	Temperature of the external face of insulation
T_{amb}:	Temperature of ambient air
T_{g1}:	Temperature of the first cover plate on the top
T_{g2}:	Temperature of the second cover in the middle

The absorber plate proves to be the elements with high hourly temperature values. It is the special component absorbing a lot of solar radiation to convert them into heat. The elements with the least temperatures are generally the glass cover justified by the presence of stagnant air layers insulating them together with their low capacity of conducting heat. It is shown that the maximum air fluid output temperatures above $50^{o}\mathrm{C}$ are generated from 12.00PM up until 7.00PM with the highest value of $74^{o}\mathrm{C}$ generated at 3.00PM owing to maximum radiation and ambient temperatures input at this time. We notice that the fluid temperatures increase lies between those of absorber and the internal insulation temperatures. These are the two parts making its pathway. Obviously, the air movement under the absorber increases heat transfer downward to the insulation part whereas the nonmoving air on its top works as an insulator for not transferring heat upward. The justification is that the convectional heat transfer coefficients for moving fluid are higher compared to stagnant air. It is also observed that before 8.00AM, both temperatures do not increase much despite the fact that they are exposed to solar radiation for 3 hours. Such observations are explained by the effect of warming up of the system by the received energy. Another remarkable observation is the high collector output temperature fluid at 7.00PM in spite of sunlight absence. This is due to the logic of mass inertia for system cooling. These results were validated to the experimental work done by [21] and to the simulation study by [13].

4.3 Parametric study on the solar air heater

4.3.1 Effect of solar collector length on the output air temperatures

The performance of the solar collector depends much on the solar intensity it captures. The higher the solar collector surface the more solar energy that is converted into heat. Even so, the surface of solar collector has to be optimized for economical and practical purpose depending on the temperatures needed. Figure 4.8 show the temperatures of the output air as function of time for various solar collector length. By periodically varying the solar collector length, its output temperatures increase but not periodically. The longer the solar collector is, the longer it takes to be heated up. The maximum output temperature for a collector of 2.5 m is $69.52^{0}\mathrm{C}$ occurring at 3PM. The maximum output for a solar collector length of 5 m is obtained at 4 PM being 93.08^{0}C. The maximum output for a solar collector length of 7 m is obtained at 5 PM being 107.11^{0}C. Lastly, the maximum output for a solar collector length of 10 m is obtained at 7 PM being 137.21^{0}C. It is noted that though longer solar collectors give high temperatures out, they are slowly heated due to their high inertia mass. Due to this effect, longer solar collectors tend to deliver their optimal output at the time of sunset. Taking account of high capitals, very long solar collector are not a good idea. In the eyes of solar drying, a solar collector between 2 and 5 may deliver enough temperatures for drying. Note that in this calculation, the velocity of air moving inside the collector is 2.5m/s.

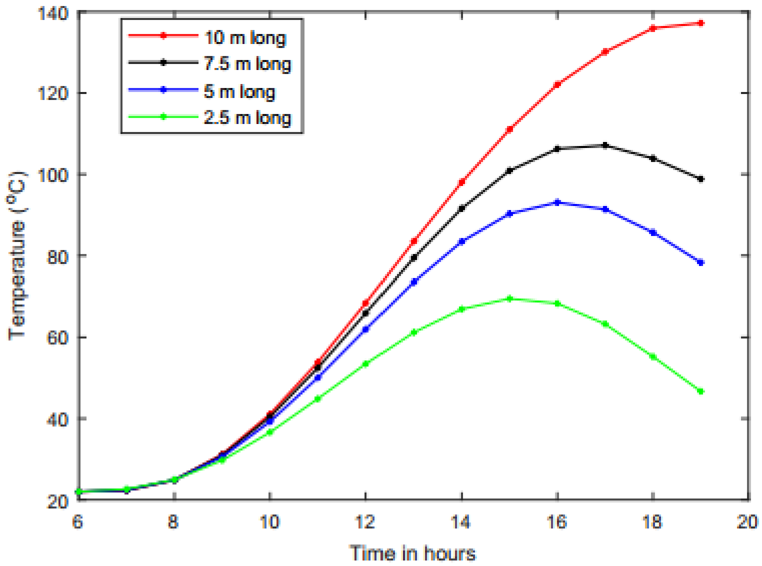

Fig. 4. 8 Effect of solar collector length variation on the air temperature output

4.3.2 Effect of the velocity on moving air inside the solar collector

The effect of the velocity of the fluid moving inside a solar collector is an important property. As it is clearly shown in figure 4.9, the air moving at 1 m/s can be heated up to 90^{0}C, that of of 2m/s can reach 74^{0}C whereby the one moving at high velocity of 3 m/s can barely be heated up to 61^{0}C. These observations are linked on the fact that the slower the air inside moves, the longer time the air takes to be heated. This effect of air moving capacity proves to be an important parameter as it can be seen that difference for the air moving at 1 m/s is higher in comparison to the air moving at a velocity of 3 m/s. Similar observation are confirmed by a single glazed conventional solar air heater [13].

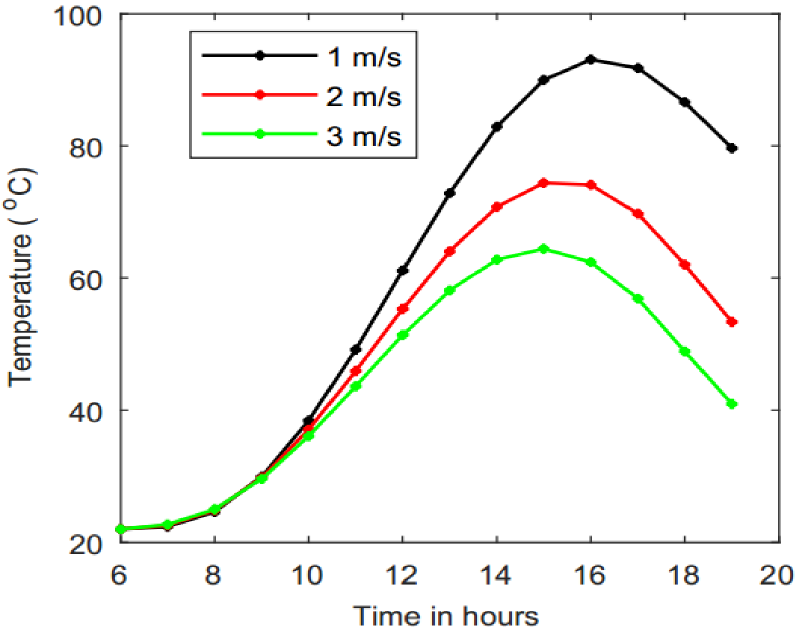

Fig. 4. 9 Influence of fluid velocity inside the collector on the air output temperature

4.3.3 Effect of some absorber materials on the solar collector performance

In designing a solar collector, the selection of absorber material is an important aspect as it is the main engine converting radiation into heat. Though it is well known that the favorable absorbers are mainly metals. For curiosity purpose this study investigates/d the use of different absorber materials depending on their properties. Three metals including aluminum, copper and steel were investigated based on thermal and optical properties shown in table 4.1. Figure 4. 10 represents the output air temperatures obtained from the analysis. In this case the absorber made in copper had e higher output in comparison with all others with a maximum output of 58.15 ^{0}C at 3.00 PM. The absorber with the lowest output temperature in this case happened to be the aluminium with the highest temperature output of

51.43. The main influential character has been the absorptivity property by analyzing the thermal properties used in Table 4.1.

Table 4. 1 Thermal and optical properties of metal used this particular calculation

Material	Specific heat (J/kg K)	Thermal conductivity (W/m K)	Density ($kg.m^{-3}$)	Absorption coefficient	Emissivity coefficient
Copper	385	389	8940	0.75	0.04
Aluminum	897	200	2700	0.54	0.04
Steel	468	46	7850	0.7	0.1

The table shows that copper absorption coefficient is the highest with a value of 0.75.The absorber in steel having the second-high output temperatures also has the second-high absorption coefficient with a value of 0.7. The aluminum on the hand has the least absorption coefficient justifying its low output in comparison to others.

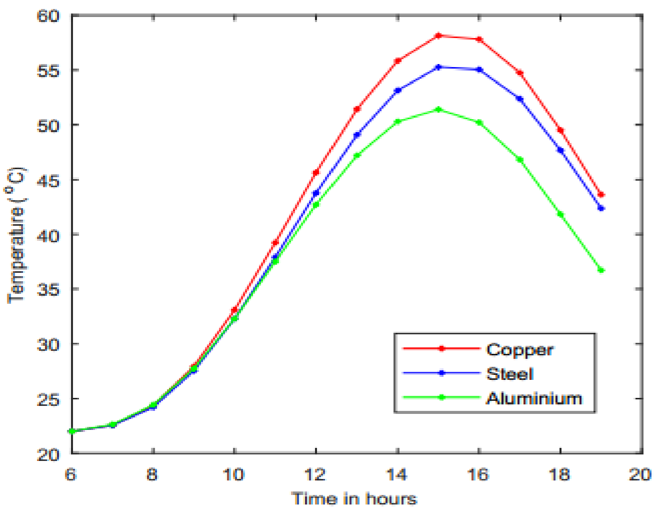

Fig. 4. 10 Effect of some absorber materials on the temperature output from the solar collector

4.3.4 Effect of using different absorber materials with same selective layer

To investigate the effect of thermal properties of absorber metals, the metals are coated with same selective layer giving them similar absorptivity and same emissivity. Table 4.2 show the absorptivity and emissivity values used for black chrome and aluminium molybdenum oxide selective layers.

Table 4. 2 Absorbers materials with selective layers optical properties

Selective layers	Materials	Absorption coefficient	Emissivity coefficient
Black chrome over nickel	▪ Aluminium ▪ Copper ▪ Steel	0.93	0.07
Aluminum molybdenum Oxide	▪ Aluminium ▪ Copper ▪ Steel	0.93	0.35

Upon the calculation, Fig.4.11 (a) and (b) are compared to investigate if there is any effect of material thermal properties. Fig. 4.11 (a) presents all the output temperatures for Aluminium, copper and steel absorbers when the selective layer of black nickel chrome over nickel is used. Different from the case in Fig.10, where aluminum is the absorber with high output of 71.44 at 15:00. The absorber in steel delivers the least output but almost equal to that of copper. The capacity of aluminium to generate higher temperatures is linked to its density. Fig. 4.11 (b) show the same case justifying that Aluminium is the best converter compared to the copper and steel absorbers. Note that this only happens in the case when all absorber materials are studied at the same emissivity and absorptivity as shown in Table 4.2. By comparing Fig.4.11 (a) and Fig 4. 11 (b) it is seen that their outputs are almost similar as for example the highest output of aluminum absorber in Fig.12 happens to 71.41 happening to be almost equal to 71.44 in Fig.11. This result may be justified based on the fact that the absorptivity coefficients for two selective layers are almost equal. It is important to notice that for both Fig.4. 11(a) and Fig.4.11 (b), the temperature output from the aluminium collector decreases quickly when there is no more radiation. The explanation found to this effect is also linked to its low density of 2700 (W/m K). By comparing its low density with copper and steel having a density of 8940 and 7850 (W/m K), it is seen that aluminium can be heated quickly compared to others. This occurrence maybe justified on the basis of energy stored formula.

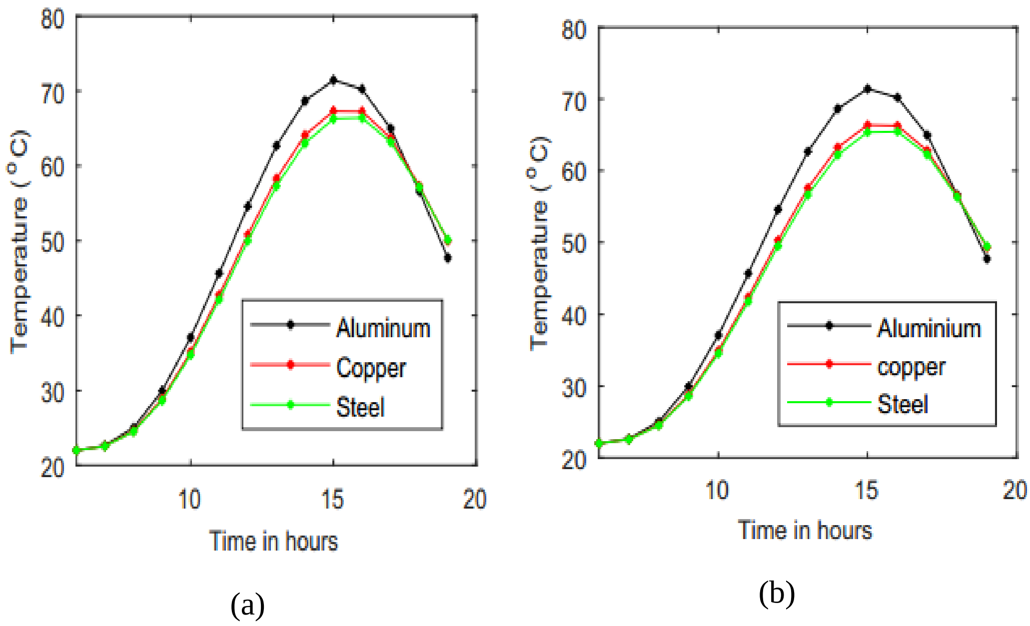

Fig. 4. 11 Comparison between absorber materials with same selective layer. (a) The selective layer is black chrome. (b) The selective layer is aluminium molybdenum oxide

4.4 Simulation results for the drying chamber

4.4.1 Temperature distribution for heated and non-heated solar dryer

The indirect solar dryer proposed in this study is designed to dry fruits and vegetables at a small traditional market ensuring the preservation of non-sold out products. For this purpose, it is believed to be working even when weather conditions are not good.

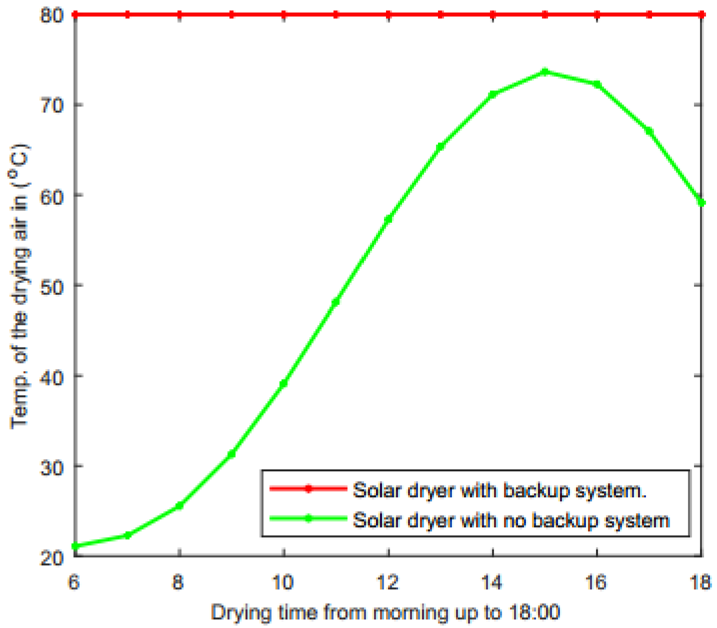

Fig. 4. 12 Drying chamber entrance temperatures for a solar dryer with a backup and for a solar dryer without backup system

To have such practical solar system, a solar dryer may be fitted with a back-up system. Such a system works at a constant temperature from morning up to night considered to be 80^0C in this study. Fig.4.12 shows its temperature deliverance at the entrance of the drying chamber in red. Note that the temperature value does not vary from morning up to night. The temperature shown in green in Fig.4.12 represents the temperatures at the entrance of the drying chamber when the system is only depending on the solar collector. It is noted that when the solar dryer has no backup, drying chamber entrance temperatures are very low in the morning.

4.4.2 Temperature distribution between trays in the drying chamber

The performance of an indirect solar dryer depends on how heat loss occurs through the drying chamber wall and also on how the temperature is distributed in various levels inside the drying chamber. Regarding the heat loss, the wall designed for our system proved to play very well the insulation role. This is justified by the fact that the temperatures at the external wall of the drying chamber are approximately equal to the ambient temperature outside and that its internal wall face temperatures approximate that of drying air temperature inside the chamber. As we have seen the distribution of ambient temperature in Fig. 4.3, we now look on the distribution of drying air temperatures between trays.

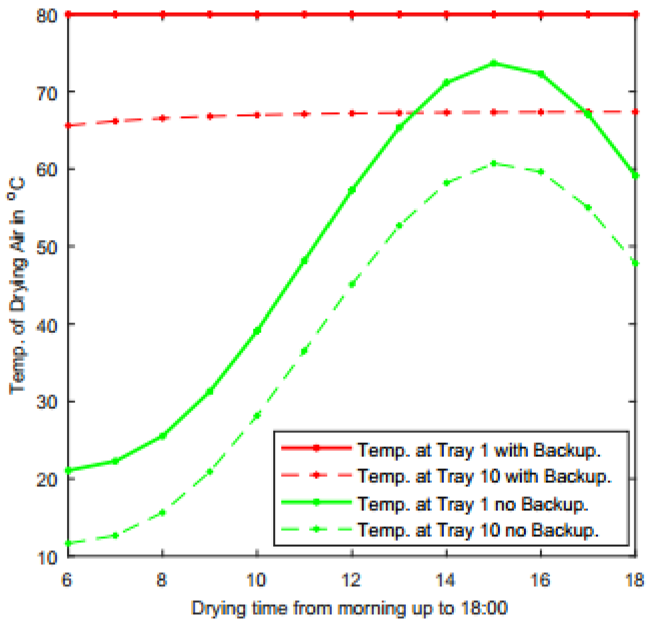

Fig. 4. 13 Difference between first tray air temperature and last tenth tray for a system with and without backup system (at U = 2 m/s, D = 5 cm; m_f = 5 kg)

Fig.4.13 indicate the difference in the air temperature distribution between first and last tenth tray. For the solar dryer working with a backup system, the distribution is shown in red curves. On the other hand, for the solar dryer without a backup system, temperature distributions are shown in green curves. In both cases of red and green curves, the drying air temperatures at tray one are higher in comparison to tray number 10 at the top shown in dashed curves. Obviously, this difference in temperature between tray 1 and tray 10 is caused by the loss in air energy as it progresses from tray 1 to tray 10. This lost energy is mainly being used to evaporate moisture from the product as the air progresses from first to the last tray [11].

4.4.3 Drying rate of solar system with a heater and without a heater

Fig.4.14 present the difference in product moisture content reduction between drying with a backup heating system and without a backup system. The presented drying curves are for products dried in the tenth tray having a specific diameter (D_f) equal to 5 cm when the drying air speed (U) equal to 2m/s. The main reason of considering the last tenth tray for this comparison is the belief that the drying process there is slow due to the effect that the temperature of drying air is low compared to the other trays.

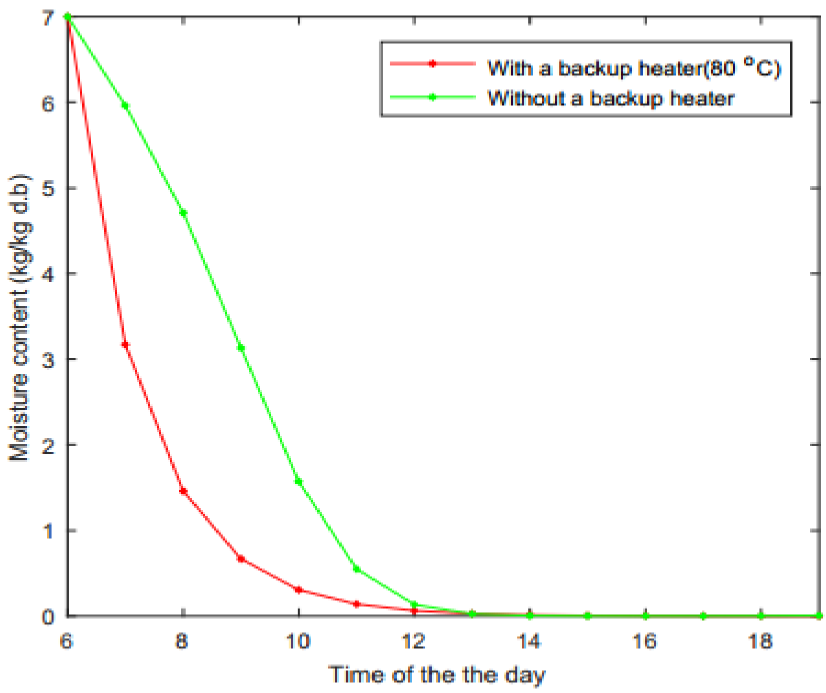

Fig. 4. 14 Effect of drying at constant and varying temperatures on the moisture content reduction (at U = 2m/s, D_f = 5 cm; tray = 10)

The red curve in Figure represent the effect of of drying with a solar collector working together with a backup system at a constant fluid temperature of 80^0C on the drying rate of pepper at the last tenth tray. On the other hand, the effect of using only the solar collector as the heating system is depicted in green curve. Obviously when drying at constant temperatures, product water removal is high from the beginning up to the end resulting in a short drying time. For the case where the drying rate is used, moisture content reduction goes very slow at the beginning corresponding to its low temperature supply in the morning time when the solar radiation reaching the collector is low. Later when much radiation intensity is gathered the moisture reduction process happen quickly. The results from calculation shows that for short drying the system with backup would require a drying time of six hours compared to 8.5 hours needed when the system is using solar air heater only. Due to that fact t, the solar radiation intermittent property using solar backup is advised especially in morning time and during night when there is no solar radiation.

4.4.4 Effect of drying at different time in the day

It is well known that drying at particular time of the day may result in a slow or faster drying process. Fig. 4.15 shows the influence of drying products at 6 am and at 11am for both a solar dryer with a heater and without a heater. For the solar dryer with heater (80^0C) shown in red curves, the difference between drying starting at six and starting at 11am is approximately 1.5 hours. The difference in drying time for the solar system without a heater is observed between 6:00am and 11:00 am drying process is approximately 2 hours. Investigating the green curves for a solar system without heater, it is seen that the change in the slope of the curve is more observable. In comparison with the drying starting at 6:00am, the slope has increased a lot for the drying process starting at 11:00am. This might be explained by the fact that the temperature of the heating air has increased. It is also seen that the drying slope for the heated system, has increased despite the fact that the drying temperature (80^0C) has not changed. This might be justified by the change in ambient air temperatures. At this time the ambient air has increased a lot and the system is already heated. Contrarily to the drying process starting at six, the air humidity is high and the systems has to be heated first. It has been noted that the drying process might not be completed if the drying process is started later than 12 am. The optimum drying time during the day for an indirect solar dryer without heating system would be between 11:00 and 18:00. At this time the ambient temperature is high, the system is already heated and much more the temperature of the heating air is higher than 48^0C. Again note that the presented drying curves are for products dried in the last tray having a specific diameter (D_f) equal to 5 cm when the drying air speed (U) equal to 2m/s. With the last tray taken due to the belief that the drying process there is slow due to the effect that the temperature of drying air is low compared to the other trays. The investigation of the difference in drying rate in different trays will be investigated by studying all different influential parameters in the last section.

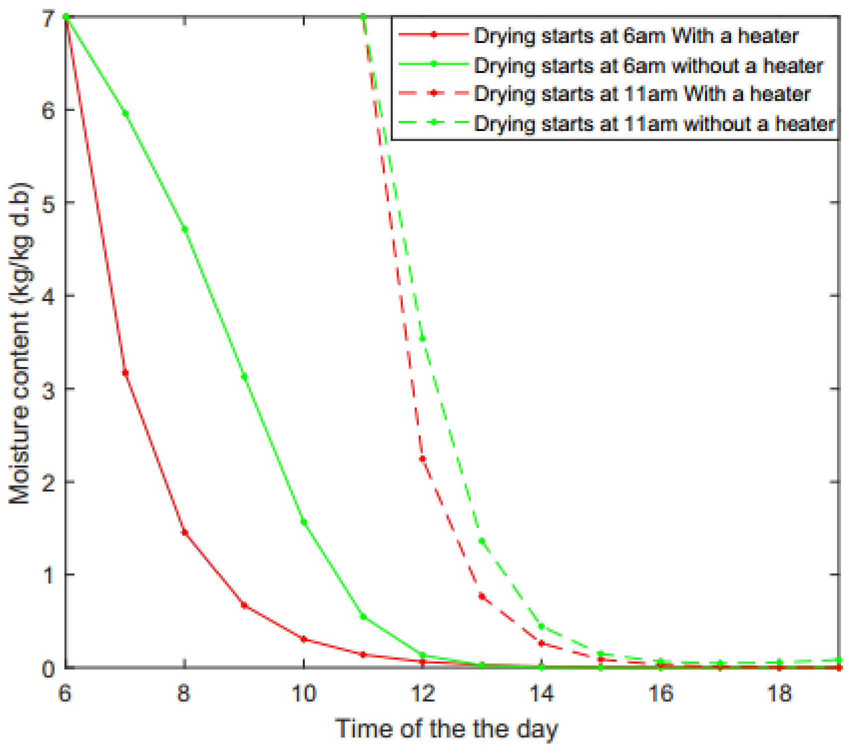

Fig. 4. 15 Effect of drying at different time of the day.

4.5 Parametric study on the drying chamber

The main parameters influencing the drying rate are inscribed in the drying rate constant in equation 3.97. These are the drying air temperature, the air velocity, product moisture content as well as the diameter (D_f) of the product. This section helps in interpreting the mathematical expressions used in chapter three into physical principles reflecting reality by investigating the influence of drying temperatures and air velocity on the drying rate of green pepper. For the purpose of having a deep feeling, the solar dryer considered in this section has a backup system allowing to tune drying air temperatures and air velocity.

4.5.1 Effect of drying air temperatures on the drying rate.

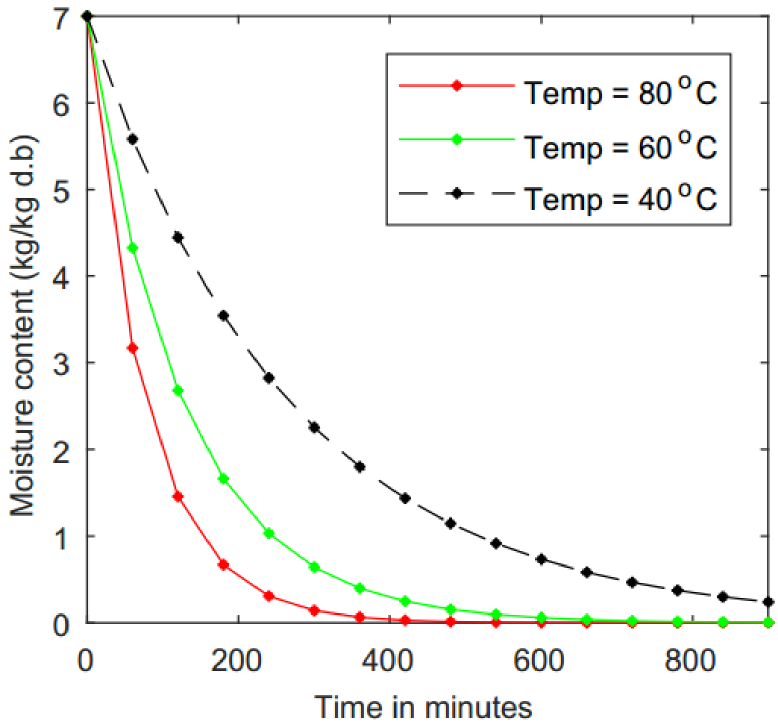

Fig. 4. 16 Effect of drying air temperature on the moisture content reduction (at 10^{th} tray, U= 2.5 m/s, D_f=5 cm;)

In drying process, temperature happen to be first main parameter influencing the drying process. The effect of this parameter on the moisture reduction is illustrated in Fig.16. Obviously drying at low temperatures lead to long drying time whereas drying at high temperatures results in short drying time. It is important to note that drying at very high temperatures in not advised as the products nature would be deteriorated. In our analysis, three constant temperatures ($40, 60 \text{ and } 80^0\text{C}$) are used to illustrate their effect on the moisture reduction rate. Note that 60 and 80^0C are in the range of the drying model derived from experiment by [18] whereas 40^0C is shown in dashed curve as it is beyond the temperature range considered during experiment. Calculations shows that drying at 80^0C occurred 3 hours earlier compared to the drying time at 60^0C happening after ten hours. Drying at 40^0C requires more than fifteen hours of drying time. These results are in accordance with the findings on drying of onions [14] and in the previous work on green pepper done by [18].

4.5.2 Effect of drying air velocity on the drying rate of green pepper

Fig. 4.17 represents the effect of drying air velocity on the drying rate of green pepper at the last tenth tray. This is also studied on the basis of product moisture reduction as a function of time. Drying at high velocity increases the capacity of water vapor capturing by the drying air. The air moving slowly the dried product speed long time around the product while fixing water at low rate whereas air moving at high velocity moves around the product and take away the evaporated vapor outside quickly. The lower the drying air is wet, the greater is the drying gradient from product inside to the surrounding air. In our study it is shown that the air moving at 5 m/s lead to the higher reduction green pepper moisture reduction whereas the reduction at 1 m/s is observed to lead to higher drying time. It is important to see that the effect of air drying temperature is very high in comparison of drying velocity effect.

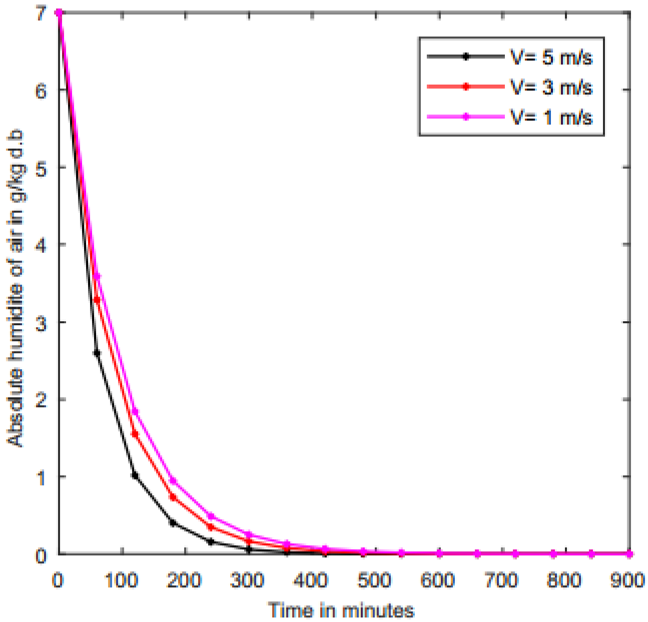

Fig. 4. 17 Effect of velocity variation on the drying rate of green pepper

(Tray =10, Tf =80^{0}C, D_f =5 cm)

4.5.3 Influence of air velocity variation on the absolute humidity of air

The properties of drying air play a very important role in drying process. As the drying air fixes more evaporated water its capacity of fixing additional water decreases. Fig. 4.18 represents the evolution in time of the drying air absolute air humidity at the last tray for when the fan in our system is operated at various air speeds. It is important to notice that the air fixes much vapor for both speeds at the starting of the drying process though it is done at a different rate. The recuperation in water vapor for the air moving at low speed is higher in comparison of the air moving at a higher speed, As a matter of fact, the air moving at 1m/s takes more time to fix much water whereas the air at 5 m/s moves quickly without fixing much. At the starting when more water evaporates, it is seen that the absolute humidity of air is higher than that of 5 m/s whereas at the end of the drying process when no more water evaporates from the products, the drying air at both speeds present same values of absolute humidity. Therefore, it is necessary that the air around the wet product is continuously replaced by a new one with higher water vapor fixing capacity moving at high velocity. In our designed system, the evaporated moist air together with the drying are pushed out by the use of a fan increasing the velocity of moving air.

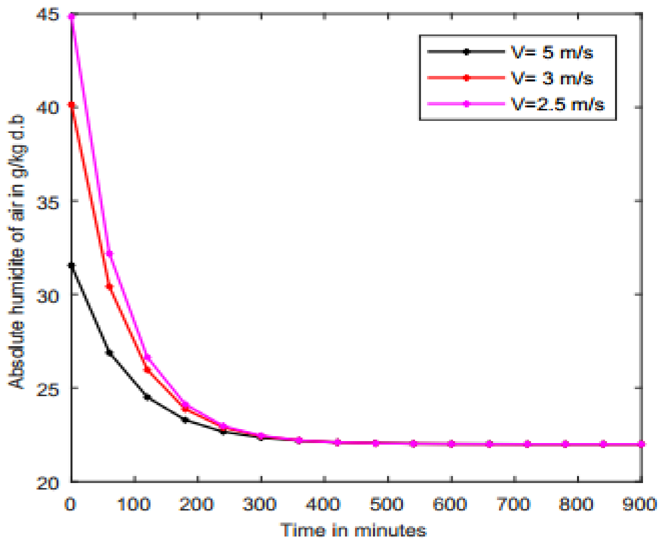

Fig. 4. 18 Influence of air velocity variation on the absolute humidity of air at the tenth tray (at T=80^{0}C D=5 cm; m=5 kg, j=10)

In solar dryer design, the decision of how long a product might take to dry is important. It helps in process forecasting and process control for good dried products. The drying rate is evaluated by the hourly reduction in product moisture content as function of drying time. A high rate in reduction in moisture reduction correspondent to the short drying time whereas slow reduction in moisture lead to long drying time. Some parameters such temperature, drying air velocity, number and position of trays together with the moving air velocity influences the length of the drying process. In the following sections, an analysis of a number of parameters is done to study their effect on the drying process of green pepper.

4.5.4 Effect of tray position on the drying rate of green pepper

As seen in the previous section, the drying air temperature at the entrance of the drying chamber is higher in comparison with drying temperature at the last tenth tray in the drying chamber. The effect of this temperature difference as well the decrease in the water vapor fixing capacity as air progresses from tray the first tray to last one lead to the difference in product drying time in various tray. This influence is illustrated in Fig.4.19 for trays 1, 5 and 10. Obviously, the drying time is in descending order from the first tray to the last one. In our calculation, the difference between the drying time between product in tray one and last tenth tray is approximately two hours. These results are in accordance with the curves trends in the work of D. Jain in [12].

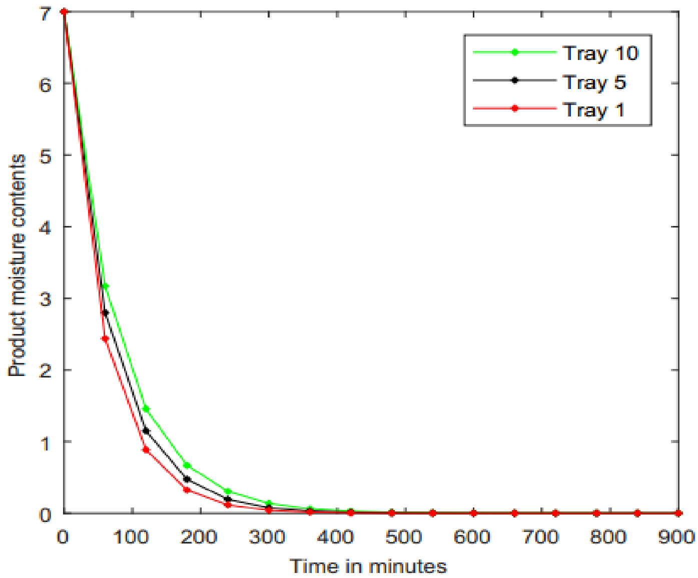

Fig. 4. 19 Variation in green pepper drying rate in the first and tenth last tray.

(U=2.5, D_f = 5 cm)

CHAPTER 5
CONCLUSION

Considering the results of the present study, the following conclusions can be made:

a. The intensity of solar radiation captured by the solar collector depends on its installation angles, sun position angles as well as the time of the day. The optimum tilt angle for solar collector in Rwanda is within a range of 0^0 and 30^0 with the optimum being 15^0. The optimum orientation angle is 0^0 which is the angle when the solar collector is facing north. On a clear day, the maximum solar radiation occurs at a time when the solar altitude angle is maximum and the azimuth angle is 0^0. This happens around 12.00 pm.
b. The ambient temperature and the solar radiation are the important parameters influencing the collector outputs temperatures. The ambient temperature observed during the day is influenced by the solar radition.
c. The observed cool ambient temperature during morning time reduces the solar collector output air temperatures. The maximum air fluid temperatures above $50^{o}\mathrm{C}$ are generated from 12.00PM until 7.00PM. The highest value of $74^{o}\mathrm{C}$ is generated at 3.00PM owing to the maximum radiation and ambient temperatures input at this time.
d. The temperature output from the solar collector is low in morning time due to the low ambient temperature and to the system heating. This suggest the use of a backup system. The optimal hours of high temperatures generation for a solar dryer without heating backup are between 11.0 am and 7.00PM. This is the optimum time for drying as the system is already heated by the sun. If the drying process is started later in the afternoon, the green pepper products won't be yet dried at the time of sunset.
e. The increase in length of the solar collector leads to the increase in collector output temperatures. It is seen that very long solar collectors spend most hours of solar radiation being heated due to their high inertial mass. It is

seen that solar collector with a length more that 5m start delivering the maximum air output at the time of sunset.

f. The speed at which the air moves inside the solar collector influences much the air output temperatures. Its increase leads to low temperature outputs.

g. The comparison done between aluminium, copper and steel absorbers show that mainly a best absorber is the one with high absorptivity coefficient. It is seen that aluminium get heated and cooled much quickly compared to copper and steel. This is due to its very low density in comparison with the density of copper and steel.

h. Inside the drying chamber, the increase of drying air velocity and air temperatures increase the water vapor fixing capacity of drying air. This effect reduces the drying rate when the air temperature and air velocity are increased.

i. The distribution in tray temperatures shows that first trays are hotter than the last ones. This difference is caused by the loss in air energy as it progresses from tray 1 to tray 10. The lost energy is mainly used to evaporate moisture from the product as it progresses. Due this temperature differences as well as the reduction in water vapor fixing capacity of air, product in tray one dries quickly compared to product in the last tray.

REFERENCES

[1] P. D. Department of Economic and Social Affairs, “World Population Prospects: The 2015 Revision, Key Findings and Advance Tables. Working Paper No. ESA/P/WP.241,” United Nations, , New York, 2015.

[2] E. D. V. Belessiotis, “Solar drying,” Solar energy, vol. 85, pp. 1665-1691, 2011.

[3] M. W., Bassey and O. G. Schimidt, “Solar drying in Africa,” International development research center, pp. 61-74, 1987.

[4] L. Bennamoun, “Reviewing the experience of solar drying in Algeria with presentation of different design aspects on solar dryers,” Renewable and Sustainable Energy Reviews , vol. 15 , p. 3371–3379, 2011.

[5] P. Om , L. Vinod , P. Anukul , K. Anil and K. Arbind , “Review on various modelling techniques for the solar dryers,” Renewable and Sustainable Energy Reviews, p. 396–417, 2016.

[6] O. Prakash and A. Kumar, Solar drying technology: Concept, Design, Testing, Modelling, Economics, and Environments, Singapore: Springer Nature Singapore Pte Ltd, 2017.

[7] Z. E. D.-K. C.T.Kiranoudis, “Equilibrium Moisture Content and heat of Desorption of Some vegetables,” Journal of Food Engineering, pp. 55-74, 1993.

[8] P. C. Phadke, P. V .Walke and V. M. Kriplani, “A review on indirect solar dryers,” ARPN Journal of Engineering and Applied Sciences, pp. 3360-3371, 2015.

[9] John A. Duffie,William A. Beckman, Solar Engineering of thermal process, New Jersey: John Wiley & Sons, 2013.

[10] D. Y. Goswami, Principles of solar engineering, Boca Raton: Taylor & Francis Group, 2015.

[11] D. Jain, “Modeling the performance of the reversed absorber with packed bed thermal storage natural convection solar crop dryer,” Journal of Food Engineering, p. 637–647, 2007.

[12] Y. Bolea, A. Grau and A. Miranda, “SDSim: A Novel Simulator for solar drying process,” Mathematical Problems in Engineering, pp. 1-25, 2012.

[13] D. Jain, “Modeling the system performance of multi-tray crop drying using an inclined multi-pass solar air heater with in -built thermal storage,” Journal of food engineering, pp. 44-54, 2005.

[14] Mohamed Yacine Nasri, Azeddine Belhamamri, “Simulation d'un sechoir solaire indirect á convection forcée pour les produits agroalimentaires,” Sciences & Technologie B, no. 44, pp. 57-62, 2016.

[15] Lyes Bennamoun, Azeddine Belhamri, “Design and simulation of a solar dryer for agriculture products,” Journal of food engineering, no. 59, pp. 259-266, 2003.

[16] R. P. Singh and D. R. Heldman, Introduction to food engineering, California: Elsevier Inc., 2009.

[17] M. Daguenet, Les séchoirs solaires: théorie et pratique, Paris: U.N.S.C.O, 1984.

[18] C. T. Kiranoudis, J. Dimitratos, Z. B. Maroulis and D. Marinos-Kouris, “State estimation in the Batch drying of foods,” DRYING TECHNOLOGY, pp. 1053-1069, 1993.

[19] C. T. Kiranoudis, Z. B.Maroulis and D. Marinos-Kouris, “Drying Kinetics of onion and green pepper,” Drying technology, pp. 995-1011, 1992.

[20] A. Belghit, M. Belahmidi, A. Bennis, B. C. Boutaleb and S. Benet, “Etude numérique d'un séchoir solaire fonctionnant en convection forcée,” Rev Gén Therm, pp. 837-850, 1997.

[21] A. A. Abood, “A comprehensive solar angles simulation and calculation using matlab,” International journal of energy and environment, vol. 6, no. 4, pp. 367-376, 2015.

[22] P. Pascal, U.Canissius, B. Germain, T. Alphonse and Pr. E. Alidina, “Study and modelisation the parameters of plate solar air collector at pingle pass for dying of Madagascar cocoabeans,” American Journal of Engineering Research (AJER), pp. 08-14, 2017.

[23] B. Amar, “Contribution a l'étude de séchage solaire de produits agricoles locaux,” Universite mentouri – constantine, Constantine, 2010.

[24] P. S. Chauhan , A. Kumar and P. Tekasakul, “Applications of software in solar drying systems: A review,” Renewable and Sustainable Energy Reviews , p. 1326–1337, 2015.

This Page Is Intentionally Left Blank

APPENDIX

APPENDIX I

Values of the physical characteristics used in the solar dryer

- Ordinary glass cover

$$Cp_g = 750 \text{ J/kg.K}$$

$$ep_v = 10 \times 10^{-3} \text{ m}$$

$$\rho_g = 2210 \text{ kg/m}^{-3}$$

$$\lambda_g = 1.3 \text{ W/m K}$$

$$\varepsilon_g = 0.9$$

- Absorber (Aluminum pent in black)

$$Cp_p = 896 \frac{J}{kg}.K$$

$$ep_n = 10^{-3} m$$

$$\rho_p = 2707 \text{ kg/m}^{-3}$$

$$\lambda_p = 205 \text{ W/m K}$$

$$\varepsilon_p = 0.96$$

- Polystyrene insulation

$$Cp_i = 1670 \text{ J/kg K}$$

$$ep_i = 4.10^{-2} m$$

$$\rho_i = 16 \text{ kg/m}^3$$

$$\lambda_i = 0.042 \text{ W/mK}$$

$$\varepsilon_i = 0.04$$

- Brick (solid brick terracotta)

$$Cp_p = 870 \text{ J/kg. K}$$

$$ep_p = 10.10^{-2}\text{m}$$

$$\rho_p = 1800 \text{ kg/m}^3$$

$$\lambda_p = 0.8 \text{ W/m. K}$$

- Dried product (Green pepper)

$$D_f = 5 \times 10^{-2} \text{ m}$$

$$X_0 = 70 \text{ \% kg/kg wb}$$

- Calculation of the absolute humidity of humid air [22]

$$W = 0.622. \frac{\varphi. P_v, \text{sat}}{P_{ah} - \varphi. P_v, \text{sat}}$$

$$P_{ah} = 1 \text{ atm}$$

$$P_{v,sat} = 10^{\left(17.433.\frac{2795}{T}.3.868 .\log_{10}(T)\right)}$$

$$\varphi = 20\% \text{ (relative humidity of air)}$$

APPENDIX II

Resolution of linear equations systems by the Gauss Seidel [22]

Iterative methods are generally preferred for large linear systems expressed in a matrix for $A \times T = B$. Among them, Gauss Seidel's method is preferred because it is easy to program, consumes less memory and converges faster.

Method of Gauss Seidel

To solve the linear system:

$$A \times T = B$$

with:

A: Square matrix of order n;

B: Column matrix;

T: Vector of unknowns;

$T = (T_1, T_2, \dots, T_n)$

Writing A in the form:

$$A = M - N$$

where:

$$M = D - L$$

$$N = U$$

with:

D: diagonal matrix

L: lower matrix

U: upper matrix

Matrix A is written as follows:

$$A = (D - L) - U$$

From an initial vector $T^{(0)}$, we can write:

$$T^{(1)} = (D - L)^{-1} \times U \times T^{(0)} + (D - L)^{-1} \times B$$

Since the inverse of (D - L) can be complicated to calculate, it is preferable to write the system as follows:

$$(D - L) \times T^{(1)} = U \times T^{(0)} + B$$

$$D \times T^{(1)} = L \times T^{(1)} + U \times T^{0} + B$$

where:

$$T^{(1)} = D^{-1} \times L \times T^{(1)} + D^{-1} \times U \times T^{(1)} \times B$$

$$T^{(k+1)} = D^{(-1)} \times L \times T^{(k+1)} + D^{-1} \times U \times T^{(k+1)} + D^{-1} \times B$$

By developing this vector recurrence, we obtain:

$$T_1^{(k+1)} = \left(B_1 - A_{11} \times T_2^{(k)} - A_{13} \times T_3^{(k)} - \ \ldots\ A_{1n}^{(k)} \times T_n^{(k)}\right)/A_{11}$$

$$T_2^{(k+1)} = \left(B_2 - A_{21} \times T_1^{(k)} - A_{23} \times T_3^{(k)} - \cdots\ A_{2n}^{(k)} \times T_n^{(k)}\right)/A_{22}$$

$$\vdots$$

$$T_n^{(k+1)} = \left(B_n - A_{n1} \times T_1^{(k)} - A_{n2} \times T_2^{(k)} - \cdots\ A_{nn-1}^{(k)} \times T_{n-1}^{(k)}\right)/A_{nn}$$

The system of these previous equations converges if:

$$\left|T_j^{(k+1)} - T_j^{(k)}\right| < \varepsilon$$

Or

$$\frac{\left|T_j^{(k+1)} - T_j^{(k)}\right|}{\left|T_j^{(k+1)}\right|} < \varepsilon$$

AUTHOR’S BIOGRAPH

The author was born in Southern Province of Rwanda on December 17th, 1990. He studied and finished his elementary school at Groupe Scolaire de Mutima in 2003. He accomplished his entire high school at Ecole des Sciences Byimana and finished in 2009. He took his undergraduate studies at the University of Rwanda and received a Bachelor of Science in Physics with honor in computational physics in 2014. After, he moved to Indonesia and studied Bahasa Indonesia for one year. In 2016, he started his master degree in the Department of Physics Engineering, Faculty of Industrial Technology at Sepuluh Nopember Institute of Technology. There, he majored in Renewable Energy Engineering with a research interest in solar thermal systems.